The osmolality-regulated mechanism of AVP neurons

and the effect of AVP on DRG glial cells

（浸透圧によるAVPニューロン調節機構とDRGグリア細胞に対するAVPの作用）

The United Graduate School of Veterinary Science,

Yamaguchi University

Taiki Moriya

2014

CONTENTS

PREFACE

Arginine vasopressin (AVP) is composed of nine amino acids and its amino acid sequence was determined in the early 1950's [69]. It is known that AVP is synthesized in the cell bodies of the magnocellular and parvocellular neurosecretory cells (MNCs and PNCs) in the supraoptic nucleus (SON) and the paraventricular nucleus (PVN) in the hypothalamus. Axons of all AVP-containing MNCs project to the neurohypophysis [42], and the release of AVP at the neurohypophysis into the systemic circulation is increased by various stimuli such as an increase in the osmolality of the extracellular fluid (ECF), a decrease in the volume of the ECF and a reduction of the blood pressure [3, 30]. Regarding increases in AVP release induced by hyperosmolality in ECF, it has been argued that MNCs themselves possess a mechanism to sense the osmolality and are capable of regulating AVP release: hyperosmolality directly activates stretch-inactivated cation (SIC) channels in MNCs in the SON due to the shift of water from the cytoplasm of MNCs to the extracellular space, thereby depolarizing MNCs to increase the action potential frequency, which, in turn increases AVP release at the neurohypophysis [48, 55, 85, 96]. The molecular identity of SIC channel in MNCs remains unclear hitherto. In the CHAPTER 1, experiments are conducted to uncover the structure and function of

molecules related to the central osmoreceptor in the SON of rats.

AVP is known to as an anti-diuretic hormone (ADH), because AVP secreted into the systemic circulation induces contraction of blood vessels and enhances water reabsorption by epithelial cells in the renal collecting duct, thereby reducing the rate of water loss and increasing blood pressure and ECF osmolality during dehydration. In addition to the role as ADH, various effects of AVP on the CNS are well established and extensively documented. In the CNS, AVP is known to be involved in stress [100], anxiety [5] and social behavioral modulations [91]. Besides the roles in the CNS, the AVP system is present and active in peripheral organs such as the heart [18], blood vessel smooth muscle cells [38, 49, 94] and also in the peripheral nervous system (PNS) [6].

In 1986, Kai-Kai *et al.* have identified AVP immunoreactivity in neurons of rat DRG [37]. Shortly later, another group characterized an accumulation of inositol phosphates in response to AVP in rat DRG [32]. From these studies, it is presumed that the AVP and AVP receptors also exists in the DRG. In the CHAPTER 2, the AVP induced responses in the rat DRG cells were investigated at the cellular and molecular level.

CHAPTER 1

Full-length transient receptor potential vanilloid 1 channels mediate calcium signals and possibly contribute to osmoreception in vasopressin neurons in the rat supraoptic nucleus

INTRODUCTION

In mammals, the osmolality of the ECF is maintained in a narrow range around 300 mosmol/kg by regulating the intake of water and salts, and the volume and concentration of urine [7]. It is generally acknowledged that ECF osmolality is monitored by the osmosensors in the CNS and PNS. AVP synthesized by MNCs in the SON and PVN of the hypothalamus is a key factor in systemic osmolality regulation. Release of AVP by MNCs in response to changes in osmolality is regulated by synaptic inputs from neurons in the Organum vasculosum lamina terminalis (OVLT) and by astroglial cells surrounding MNCs. Hyperosmolality increases the action potential frequency in OVLT neurons, which send glutamatergic excitatory signals to MNCs [7, 72, 96]. Astrocytes in the SON are reported to secrete taurine in response to hypoosmolality [20]. Taurine released in the SON activates glycine receptors in MNCs, thereby hyperpolarizing these neurons to reduce action potential discharge. In addition to the osmosensing mechanisms in the central nervous system (CNS), the osmosensors also operate in the periphery. Injection of hyperosmotic saline via stomach tube stimulated AVP release that involved activation of osmoreceptors in splanchnic nerves [13]. These receptors are located in the mesentery of the upper small intestine [13] and in the portal vein [93]. The appropriate afferent signals

reach MNCs through the spinal cord and ascending tracts.

Besides the osmosensory mechanisms mentioned above, as written in PREFACE, it has been argued that MNCs sense changes in the osmolality of the ECF by the osmoreceptors expressing on its cell membrane. The osmoreceptor in the MNCs in the SON is called SIC channels. The molecular nature of SIC channels in MNCs remains unclear. In the PNS, the osmoreceptors were identified as TRPV4 channels, these being a subtype of the transient receptor potential (TRP), non-selective cation channel superfamily [46]. For the MNCs it has been demonstrated that neurons isolated from mice lacking *Trpv1* showed no osmoreceptive SIC currents in response to hyperosmolality [80]; in the same study it has also been reported that no signal for the N-terminal portion of *Trpv1* was detected at mRNA (RT-PCR) and protein (immunohistochemistry) levels. Subsequently it was shown that MNCs from a wild type mice did not respond to the TRPV1 agonist, capsaicin, while SIC currents were blocked by the non-selective TRPV antagonist, ruthenium red (RR), but not by the selective TRPV1 antagonist, capsazepine (CPZ). From these results, it has been suggested that N-terminal variants of *Trpv1* have a crucial role in generating the SICs that underlies osmoreception in AVP neurons [80]. In the OVLT, TRPV4 was initially suggested to be a plausible candidate for the osmoreceptor in the

CNS [50, 57], but more recent study using *Trpv1*-knock-out mice revealed the involvement of TRPV1 in the osmoreception of OVLT neurons [15].

The purpose of the present study was to uncover the structure and function of molecules related to the central osmoreceptor in the SON of rats. For this purpose, we performed RT-PCR and immunohistochemistry for TRPV1-related molecules, and measured electrophysiological parameters in rat SON neurons in response to osmolality changes and TRPV-related drugs. Since it has been reported that the SIC channel is highly permeable to Ca^{2+}, and reductions in cell volume caused increases in the cytosolic Ca^{2+} concentration ($[Ca^{2+}]_i$) in rat SON neurons [104], we have also used the fura-2-based $[Ca^{2+}]_i$ imaging technique to analyze those responses. We used transgenic rats carrying cell-specific fluorescent markers i.e. AVP-eGFP [92, 98] and oxytocin (OT)-mRFP rats [19], to readily distinguish between the two types of neurons residing in the SON.

MATERIALS AND METHODS

Cell isolation

SON neurons were isolated from brain tissues containing the SON of young male Wistar rats weighing about 50g (3-4 weeks old), which were housed at 23–24˚C under a 12 h of light (07h00 to 19h00) and 12 h of darkness cycle. To differentiate AVP and OT neurons, two types of male Wistar transgenic rats, AVP-eGFP [92, 98] and OT-mRFP rats [19], (3-4 weeks old) were also used. These transgenic rats used in the experiments were bred in the Institute of Experimental Medicine of the Academy of Sciences of the Czech Republic (IEM-AS CR) animal facility (project experiment license #CZ 205/2010/2013). All experiments were carried out under the control of the Ethics Committee of Animal Care and Experimentation, Tottori University, Japan and in accordance with the European Communities Council Directive of 24 November 1986 (86/609/EEC) regarding the use of animals in research and the use of transgenic rats were approved by the Ethics Committee of the IEM-AS CR, Prague, Czech Republic. SON neurons were acutely dissociated by enzymatic and mechanical treatments of the tissues as described previously [41, 75], with minor modifications. In brief, 6-8 blocks of basal hypothalamic SON tissues (1 mm long, 1 mm thick, 1 mm wide) were dissected under a microscope. The tissues were enzymatically

dissociated by incubation in oxygenated HEPES-buffered normal Locke's (NL; in mM: 140 NaCl, 5 KCl, 2 $CaCl_2$, 1 $MgCl_2$, 10 glucose, 10 HEPES, pH was adjusted to 7.4 with Tris) solution supplemented with 1 mg/ml deoxyribonuclease I, 0.5 mg/ml protease X, and 0.5 mg/ml protease XIV (all from Sigma-Aldrich, St Louis, MO, USA). After incubation, tissues were washed with NL and triturated with a silicon-coated Pasteur pipette to isolate SON cells. Cells were plated onto coverslips (11 mm in diameter, 0.12 mm thick) or plated onto 22 mm, 0.17 mm thick glass-bottom dishes (WillCo Wells Dishes-BV, Amsterdam, Netherlands).

Electrophysiology

Ion currents were measured with standard whole-cell voltage clamp techniques, as described previously [24]. Recording pipettes were pulled from glass capillaries (GD-1.5, Narishige, Tokyo, Japan) by a framed puller (P-97, Sutter, Novato, CA, USA). Pipettes with 2.5-5 MΩ tip resistance when filled with the KCl-based pipette solution composed of (in mM): 135 KCl, 1 $MgCl_2$, 10 Hepes, 1.6 EGTA, 10 D-glucose, 3 Na_2ATP (pH was adjusted to 7.3 with Tris) were used. Cells were continuously perfused with the NL at a flow rate of 1 ml/min by gravity and overflow solution was removed with an electronic

pump. An agar bridge containing 2% agar and 154 mM NaCl in conjunction with an Ag-AgCl wire was used as the reference electrode. Since liquid-junction potentials between the bath and pipette solutions were measured to be less than ±3 mV, they were not corrected. The patch-clamp amplifier used was an Axopatch 200A (Axon Instrument, USA). Membrane potentials were controlled and whole-cell currents were sampled and stored with dedicated software (Axograph, Berkeley, CA, USA) running on a Macintosh computer (Apple, Cupertino, CA, USA).

Action potential frequency was measured in the on-cell configuration of the patch-clamp technique with an Axopatch 200A amplifier. The currents reflecting action potentials were continuously recorded at a sampling frequency of 40 kHz throughout the experiments by a personal computer (Macintosh, Apple, Cupertino, CA, USA) in conjunction with an analog/digital converter (Power Lab, AD Instruments, Castle Hill, NSW, Australia). The data were analyzed by a Labchart software (AD Instruments, Castle Hill, NSW, Australia) and the spike frequency was calculated from numbers of spikes recorded during 30 sec before and during mannitol application. The NL and the KCl-based pipette solution were used as perfusion and intrapipette solutions, respectively, in the action potential measurements.

Stored data were analyzed by IGOR Pro software (WaveMetrics, Portland, OR, USA). Data are presented as mean ± SEM (n = the number of cells). Statistical significance was assessed by a Student's t-test and ANOVA. Differences were considered statistically significant if $P < 0.05$.

$[Ca^{2+}]_i$ measurements

The $[Ca^{2+}]_i$ in SON neurons was measured with a fluorescent Ca^{2+} indicator Fura-2 according to the procedure reported previously [65]. The dissociated SON cells were incubated in NL containing 2 μM Fura-2/AM (Merck, Whitehouse Station, NJ, USA) and 0.01% Pluronic acid F-127 (Life technologies, Carlsbad, CA, USA) for 60 min at room temperature (22-24ºC) in the dark. After incubation, the coverslip was mounted onto the recording chamber (RC-25F, Warner Instruments, Hamden, USA) which is fixed on the stage of an inverted fluorescence microscope (IX71, Olympus, Tokyo, Japan). The cells were continuously perfused with solutions containing various experimental drugs through polypropylene tubes connected to a peristaltic pump (Minipuls 3, Gilson, Middleton, WI, USA) at a flow rate of 1.4 ml/min. In this system, the solution around the cells could be changed rapidly within a few seconds. The Fura-2 fluorescence signal was detected

through a UV objective lens (UApo 20×3/340, Olympus, Tokyo, Japan), and the florescence images passing through a band-pass filter (500 ± 10 nm) were captured by a cooled CCD camera (ORCA-ER, Hamamatsu Photonics, Shizuoka, Japan).

Fura-2 images were captured at a sampling frequency of 0.2 Hz using Aqua Cosmos software (Hamamatsu Photonics, Shizuoka, Japan). The fluorescent intensity (F) at excitation wavelengths of 340 nm (F340) and 380 nm (F380) was determined by analysis software (Aqua Cosmos, Hamamatsu Photonics). The ratio of fluorescence for each pixel obtained with excitation at 340 and 380 nm (*F340/F380*) was used to calculate $[Ca^{2+}]_i$. A calibration curve of $[Ca^{2+}]_i$ for *F340/F380* was determined using a series of Ca^{2+}-buffered solutions (Life technologies, Carlsbad, CA, USA). To estimate the $[Ca^{2+}]_i$ levels in individual cells, regions of interest (ROIs) were chosen to include the soma of each SON cell, and average values for $[Ca^{2+}]_i$ in pixels contained in each ROI were calculated. The amplitude of $[Ca^{2+}]_i$ responses was expressed as $\Delta[Ca^{2+}]_i$, which was calculated by subtracting average $[Ca^{2+}]_i$ levels during 30 sec before mannitol or capsaicin application from the peak $[Ca^{2+}]_i$ amplitudes detected during 3 min after the onset of mannitol or capsaicin application. Only SON neurons showing a low baseline and responding to high K^+ with a rapid and large (>300 nM) increase in $[Ca^{2+}]_i$ were used for analysis in the

present study.

For $[Ca^{2+}]_i$ measurements on SON neurons obtained from AVP-eGFP-positive and OT-mRFP-positive transgenic rats, neurons were visualised and identified under a fluorescence microscope (AxioObserver.D1, Zeiss, Jena, Germany) equipped with a motorized carousel with filters for monitoring GFP and RFP fluorescence, and an epifluorescence oil immersion objective (FLUAR 40X/1.3 oil and FLUOR 20X0.75, Zeiss, Jena, Germany). The fluorescence intensity was detected by using a cooled CCD camera (AxioCam MRm, Zeiss, Jena, Germany) and the whole system was controlled by Zeiss ZEN Imaging software (2012-SP2/AxioVision SE64 Rel. 4.8.3). The fluorescence intensity was measured with excitations at 340 and 380 nm, and emission at 510 nm. $[Ca^{2+}]_i$ values from these experiments were expressed as the fluorescence ratio, *F340/F380* after photo-bleaching compensation. The control and test solutions were applied using a multiple capillary perfusion system (200 μm inner diameter capillary tubing, flow rate 250 μl/min) and the cells were subjected to a constant fast flow control buffer. Each capillary was fed by a reservoir 50 cm above the bath and connected to a temperature control device (Model: TC-324B; Harvard-Paris, France).

Changes in the calculated $[Ca^{2+}]_i$ or the *F340/F380* ratio were analyzed by IGOR Pro

(WaveMetrics, Portland, OR, USA) and Excel (Microsoft, Redmond, WA, USA). Ratio responses exceeding 4xSD of the baseline noise level for longer than 15 s were considered to be a meaningful in this series of experiments. Data are presented as means ± SEM. The statistical significance was assessed by One-factor analysis of variance (ANOVA) or a Student's *t*-test. Differences were considered statistically significant if $P < 0.05$.

Immunohistochemistry

The whole brain was dissected from rats killed by guillotine under deep anesthesia (pentobarbital, 50 mg/kg B.W., i.p.). Paraformaldehyde (PFA)-fixed and paraffin-embedded tissue sections prepared from small pieces (5-8 mm square) of brains containing the SON region were subjected to immunofluorescence staining. Tissue sections of 5-μm thickness were boiled (96-98 ºC) in a citrate buffered solution (pH = 6.2) for 20 min to activate antigen and blocked with PBS supplemented with 2 % skim milk (blocking solution) for 30 min. After the blocking process, tissue sections were incubated with primary antibodies. The primary antibodies used were a goat anti-TRPV1 polyclonal antibody directed against the N-terminal portion of TRPV1 [22] (1:50 dilution; Cat# sc-12498; Santa Cruz Biotechnology, Dallas, TX, USA), a rabbit anti-AVP polyclonal

antibody (1:500 dilution; Cat# 061461-1; Bachem AG, Bubendorf, Switzerland) and a rabbit anti-OT polyclonal antibody (1:500 dilution; Cat# T-4084; Bachem AG, Bubendorf, Switzerland). These primary antibodies were diluted at desired concentrations with a blocking solution. Tissue sections were incubated in the presence of the anti-TRPV1 antibody and anti-AVP antibody, or in the presence of the anti-TRPV1 antibody and anti-OT antibody at 4 ºC for 12 h. After washing out the primary antibodies with PBS, tissue sections were incubated with secondary antibodies for 1 h in the dark. The secondary antibodies used were Alexa Fluor 633-conjugated donkey anti-goat IgG antibody for the anti-TRPV1 antibody and Alexa Fluor 488-conjugated donkey anti rabbit IgG antibody for the anti-AVP and OT antibodies. Both secondary antibodies were diluted at 1:500 with a blocking solution. The stained sections were mounted in a glycerol-based mounting solution supplemented with 1.4-dyazabicycro [2,2,2] octane (Sigma-Aldrich, St Louis, MO, USA) at 2.5 %. Fluorescence images were captured by a laser confocal microscope (FV10i; Olympus, Tokyo, Japan) through a 20X objective lens with an image resolution of 1024 x 1024.

RNA isolation and reverse transcription-polymerase chain reaction (RT-PCR)

Total RNAs used for RT-PCR were isolated from SON and dorsal root ganglia (DRG) using Trizol reagent (Life technologies, Carlsbad, CA, USA) according to the manufacture's protocol. Reverse transcription was performed with 2 μg total RNAs and an oligo dT primer using SuperScript^{TM} III Reverse Transcriptase (Life technologies, Carlsbad, CA, USA) according to the manufacture's protocol. PCR was performed with 1μl of first-strand cDNA, a primer pair listed in Table 1 and Emerald Amp MAX PCR Master Mix (Takara Bio, Shiga, Japan). The PCR profile was as follows: 94 ºC for 30 seconds, 54 ºC for 30 seconds and 72 ºC for 160 seconds, for 35 cycles.

Table 1. Individual TRPV1 primers for RT-PCR

Product name	Sources[a]	Primer codes	Sequence (5' - 3')	Predicted length
Full-length Trpv1	NM_031982	TRPV1-N	ATGGAACAACGGGCTAGCTTAGACT	2514 bp
		TRPV1-C	TTCTCCCCTGGGACCATGGAATCC	
Trpv1	NM_031982	ex04F	GACAGACAGCCTGAAGCAGT	740 bp
		ex08R	ATCTGTCCCACTTGTCCTGT	
Trpv1b	AB041029	ex04F	GACAGACAGCCTGAAGCAGT	560 bp
		ex08R	ATCTGTCCCACTTGTCCTGT	
VR.5'sv	AF158248	5'SV-ex06F	CCAATCATCCAGGGACTAGC	426 bp
		ex08R	ATCTGTCCCACTTGTCCTGT	
$Trpv1_{VAR}$		ex04F	GACAGACAGCCTGAAGCAGT	841 bp
		ex08R	ATCTGTCCCACTTGTCCTGT	
Stretch-inhibitable nonselective cation channels	AB015231	5'SV-ex06F	CCAATCATCCAGGGACTAGC	605 bp
		ex08R	ATCTGTCCCACTTGTCCTGT	
GAPDH	NM_017008	GAPDH-F	AGTCGGAGTGAACGGATTTGG	488 bp
		GAPDH-R	AGTTGTCATGGATGACCTTGG	

Stretch-inhibitable nonselective cation channels	AB015231	5'SV-ex06F	CCAATCATCCAGGGACTAGC	1825 bp
		TRPV4-C	CAGTGGTGCGTCCTCCGCCCT	
Trpv1_SON	LC008303	5'SV-ex06F	CCAATCATCCAGGGACTAGC	2087 bp
		TRPV1-C-end	ATGTGTCCAAGTAGAGATTTGCCAT	

[a]Sources were described by the accession number in GenBank

After amplification, PCR products and a 200 bp (Takara Bio, Shiga, Japan) or 100 bp DNA ladder (New England Biolabds, Ipswich, MA, USA) were electrophoresed with TAE buffer on 1.5% agarose gel (NIPPON GENE CO., LTD Tokyo, Japan) containing 1 μg/ml ethidium bromide. Bands were excited by ultraviolet light and photographed. PCR products with the primer set as TRPV1-N & TRPV1-C and 5'sv-ex06F & TRPV1-C-end were confirmed by sequencing using an ABI 3130 Genetic Analyser (Life technologies, Carlsbad, CA, USA) with primers for DNA sequencing (Table 2 and 3).

Table 2. Primers for full-length *Trpv1* sequencing

Primer Codes	Sequence (5' - 3')	Position
TRPV1-N	ATGGAACAACGGGCTAGCTTAGACT	81-115
ex04F	GACAGACAGCCTGAAGCAGT	626-645
ex07F	CACCTATCCAGGAAGTTCAC	1170-1189
ex11F	ATGGTGTTCTCCCTGGCCAT	1701-1720
ex13F	AGAACATCTGGAAGCTGCAG	2161-2180
TRPV1-C	TTCTCCCCTGGGACCATGGAATCC	2569-2594

Table 3. Primers for *Trpv 1_SON* sequencing

Primer Codes	Sequence (5' - 3')	Position
ex07F	CACCTATCCAGGAAGTTCAC	409-429
ex08R	ATCTGTCCCACTTGTCCTGT	585-605
ex11F	ATGGTGTTCTCCCTGGCCAT	940-960
ex13F	AGAACATCTGGAAGCTGCAG	1400-1420
TRPV1-C-end	ATGTGTCCAAGTAGAGATTTGCCAT	2062-2087

Solutions and drugs

A solution containing high K^+ (50 mM) was made by the isotonic replacement of Na^+ of the NL solution with K^+. A Ca^{2+}-free solution was made by omitting $CaCl_2$ from the NL solution. According to the suppliers' instructions the concentrated stock solutions were prepared with appropriate solvents (dry DMSO, dH_2O), capsaicin (Sigma-Aldrich, St Louis, MO, USA), an agonist of TRPV1, at 1 mM; capsazepine (CPZ) and N-(4-tertiarybutylphenyl)-4-(3-cholorphyridin-2-yl)tetrahydropyrazine-1(2H)-carbox-amide (BCTC) (Sigma-Aldrich, St Louis, MO, USA), antagonists of TRPV1, at 10 mM; ruthenium red (Sigma-Aldrich, St Louis, MO, USA), an antagonist of TRPV, at 10 mM; tetrodotoxin (Nacalai Tesque, Kyoto, Japan), an inhibitor of voltage gated Na^+ channels, at 1 mM were dissolved and stored at -30˚C until use. The osmolality of the NL solution and the NL solution containing 50 mM mannitol was measured with an osmometer (VAPRO 5520, WESCOR, Logan, Utah, USA): the former was 298 ± 6 mosmol/kg（n = 5）and the latter, 329 ± 5 mosmol/kg (n = 3).

RESULTS

RT-PCR and sequencing of Trpv1-related molecules

First, we performed RT-PCR to examine the mRNA expression of *Trpv1*-related molecules in the SON of rats. Supplemental Tables 1 and 2 show the primer sequences used in this study. As for *Trpv1*-related molecules in rat, four splice variants have been reported to date (Fig. 1A). *Trpv1b*, which lacks exon 7; *VR.5'sv,* which lacks exons 1 - 4 and 7, and contains a sequence consisting of exons 5 and 6 with a part of introns 4 and 5 in the 5' terminal portion [77]; $Trpv1_{VAR}$, which lacks exon 1 and a part of exon 16, and contains the same sequences before exons 6 as *VR.5'sv* [90]; and *stretch-inhibitable nonselective cation channels* found in the kidney[86], which lacks exons 1 - 5 and contains the same intron sequences before exons 6 as *VR.5'sv* and replaced 3 exons of 3' region with 3' region of *Trpv4*. To examine which molecules are expressed in the SON, two sets of primer pairs, ex04F & ex08R and 5'SV-ex06F & ex08R, were used to distinguish the four variants and the *Trpv1*. A band around 740 bp was detected using the primer set of ex04F & ex08R (Fig. 1B). The size of this PCR product corresponds to that from full-length *Trpv1* cDNA. A subtle band

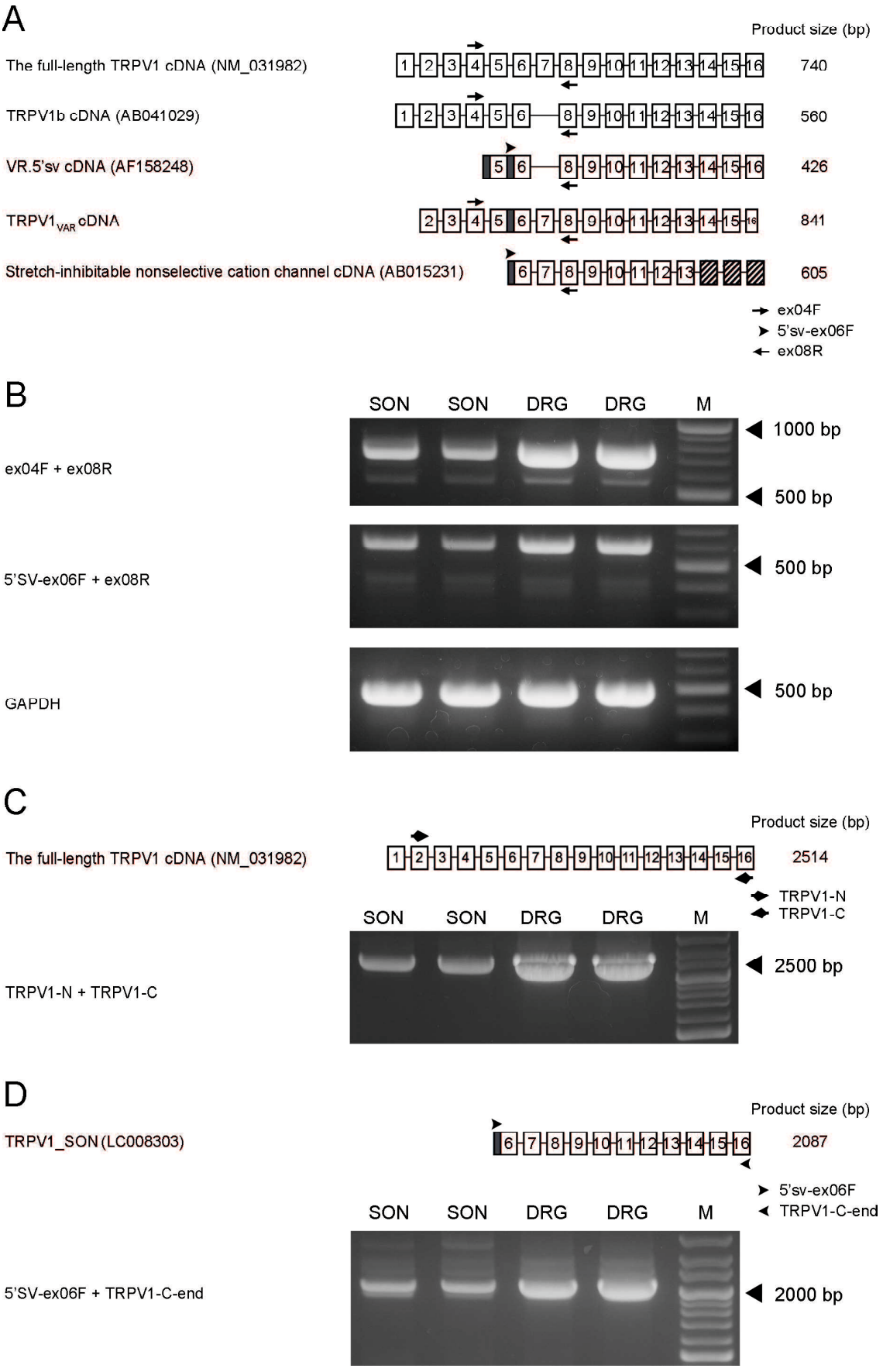
A
Product size (bp)
The full-length TRPV1 cDNA (NM_031982)
740
TRPV1b cDNA (AB041029)
560
VR.5'sv cDNA (AF158248)
426
TRPV1VAR cDNA
841
Stretch-inhibitable nonselective cation channel cDNA (AB015231)
605
ex04F
5'sv-ex06F
ex08R
B
SON
SON
DRG
DRG
M
ex04F + ex08R
1000 bp
500 bp
5'SV-ex06F + ex08R
500 bp
GAPDH
500 bp
C
Product size (bp)
The full-length TRPV1 cDNA (NM_031982)
2514
TRPV1-N
TRPV1-C
SON
SON
DRG
DRG
M
TRPV1-N + TRPV1-C
2500 bp
D
Product size (bp)
TRPV1_SON (LC008303)
2087
5'sv-ex06F
TRPV1-C-end
SON
SON
DRG
DRG
M
5'SV-ex06F + TRPV1-C-end
2000 bp

Fig. 1. RT-PCR analysis of *Trpv1* mRNAs expressed in the supraoptic nucleus (SON) and the dorsal root ganglion (DRG).

The total RNAs from the SON and the DRG were reverse transcribed, and amplified by PCR with each primer pair described in Supplemental Table 1. Primers for a house keeping gene, *glyceraldehyde 3-phosphate dehydrogenase (GAPDH)*, were used as an internal standard and generated a 450 bp fragment. Amplification products were electrophoresed on 1.5 % agarose gel and visualized by ethidium bromide. Lane M, DNA marker. (A) Compositions of exons of TRPV1-related molecules. The numbers in the squares represent the exon number for full-length *Trpv1* shown at the top. The arrow heads and arrows represent 5' and 3' primers. The expected sizes of the PCR products amplified with each primer pair is shown on the right. The filled squares represent the intron region of *Trpv1*. The nucleotide sequence in the 3' region of the exon composition of the '*stretch-inhibitable nonselective cation channel* (shown as hatched squares) is identical to the sequence of the 3 exons of the 3' region of *Trpv4*. (B) Results of RT-PCR for 5' regions of *Trpv1*-related molecules expressed in the SON and the DRG. (C) Results of RT-PCR for full-length TRPV1 in the SON and the DRG. (D) Results of RT-PCR for a new N-terminal splice variant of TRPV1 in the SON and the DRG.

around 560 bp was also detected and its size corresponds to *Trpv1b*. In addition, a band around 600 bp was detected using the primer set of 5'SV-ex06F & ex08R. The size corresponds to *stretch-inhibitable nonselective cation channels* cDNA found in the kidney. As a control, total RNAs from the DRG were used for RT-PCR, with which similar molecules were detected compared to those from SON.

We next confirmed the expression of full-length *Trpv1* in the SON by RT-PCR using the primer pairs of TRPV1-N & TRPV1-C, which amplify the 5' and 3' ends of the open reading frame of *Trpv1* (Fig. 1C). A single band around 2500 bp, which is close to the size of full-length *Trpv1*, was detected. We then identified this PCR product by direct sequencing. Two distinct nucleotide sequences were obtained: one was identical to the sequence reported for rat *Trpv1* (NM_031982), and the other was with three substitutions of the nucleotides: G134T, C367A, and C1400T. PCR products using cDNA from DRG tissues with the same primer pairs TRPV1-N & TRPV1-C were also sequenced, and the sequences were identical to those of the SON.

We also examined whether the 600 bp molecule is *stretch-inhibitable nonselective cation channels* found in the kidney using specific primers (5'SV-ex06F & TRPV4-C). We could not detect PCR products corresponding to *stretch-inhibitable nonselective cation*

channels (data not shown), instead we observed a specific band around 2000 bp when we used primers 5'SV-ex06F & TRPV1-C-end (Fig. 1D). The sequence of the PCR product (*Trpv1_SON*, NCBI Accession No. LC008303) does not match known TRPV1-related molecules reported hitherto (Fig. 2).


1
TRPV1 (NM_031982) cagctccaag gcacttgctc catttggggt gtgcctgcac ctagctggtt gcaaattggg ccacagagga
TRPV1_SON (LC008303) ---------- ---------- ---------- ---------- ---------- ---------- ----------
71
140
TRPV1 (NM_031982) tctggaaagg atggaacaac gggctagctt agactcagag gagtctgagt ccccacccca agagaactcc
TRPV1-N
TRPV1_SON (LC008303) ---------- ---------- ---------- ---------- ---------- ---------- ----------
141
210
TRPV1 (NM_031982) tgcctggacc ctccagacag agaccctaac tgcaagccac ctccagtcaa gccccacatc ttcactacca
TRPV1_SON (LC008303) ---------- ---------- ---------- ---------- ---------- ---------- ----------
211
280
TRPV1 (NM_031982) ggagtcgtac ccggcttttt gggaagggtg actcggagga ggcctctccc ctggactgcc cttatgagga
TRPV1_SON (LC008303) ---------- ---------- ---------- ---------- ---------- ---------- ----------
281
350
TRPV1 (NM_031982) aggcgggctg gcttcctgcc ctatcatcac tgtcagctct gttctaacta tccagaggcc tggggatgga
TRPV1_SON (LC008303) ---------- ---------- ---------- ---------- ---------- ---------- ----------
351
420
TRPV1 (NM_031982) cctgccagtg tcaggccgtc atcccaggac tccgtctccg ctggtgagaa gcccccgagg ctctatgatc
TRPV1_SON (LC008303) ---------- ---------- ---------- ---------- ---------- ---------- ----------
421
490
TRPV1 (NM_031982) gcaggagcat cttcgatgct gtggctcaga gtaactgcca ggagctggag agcctgctgc ccttcctgca
TRPV1_SON (LC008303) ---------- ---------- ---------- ---------- ---------- ---------- ----------
491
560
TRPV1 (NM_031982) gaggagcaag aagcgcctga ctgacagcga gttcaaagac ccagagacag gaaagacctg tctgctaaaa
TRPV1_SON (LC008303) ---------- ---------- ---------- ---------- ---------- ---------- ----------
561
630
TRPV1 (NM_031982) gccatgctca atctgcacaa tgggcagaat gacaccatcg ctctgctcct ggacgttgcc cggaagacag
ex04F
TRPV1_SON (LC008303) ---------- ---------- ---------- ---------- ---------- ---------- ----------
631
700
TRPV1 (NM_031982) acagcctgaa gcagtttgtc aatgccagct acacagacag ctactacaag ggccagacag cactgcacat
TRPV1_SON (LC008303) ---------- ---------- ---------- ---------- ---------- ---------- ----------
701
770
TRPV1 (NM_031982) tgccattgaa cggcggaaca tgacgctggt gaccctcttg gtggagaatg gagcagatgt ccaggctgcg
TRPV1_SON (LC008303) ---------- ---------- ---------- ---------- ---------- ---------- ccaatcatcc
1 10

```
                      771                                                                                  840
TRPV1 (NM_031982)     gctaacgggg acttcttcaa gaaaaccaaa gggaggcctg gcttctactt tggtgagctg cccctgtccc

TRPV1_SON (LC008303) agggactagc ctcatttgtg gggctccact ggggatcctg tgttggctgc aggtgagctg cccctgtccc
                      11                                                                                   80

                      841                                                                                  910
TRPV1 (NM_031982)     tggctgcgtg caccaaccag ctggccattg tgaagttcct gctgcagaac tcctggcagc ctgcagacat

TRPV1_SON (LC008303) tggctgcgtg caccaaccag ctggccattg tgaagttcct gctgcagaac tcctggcagc ctgcagacat
                      81                                                                                  150

                      911                                                                                  980
TRPV1 (NM_031982)     cagcgcccgg gactcagtgg gcaacacggt gcttcatgcc ctggtggagg tggcagataa cacagttgac

TRPV1_SON (LC008303) cagcgcccgg gactcagtgg gcaacacggt gcttcatgcc ctggtggagg tggcagataa cacagttgac
                      151                                                                                 220

                      981                                                                                 1050
TRPV1 (NM_031982)     aacaccaagt tcgtgacaag catgtacaac gagatcttga tcctgggggc caaactccac cccacgctga

TRPV1_SON (LC008303) aacaccaagt tcgtgacaag catgtacaac gagatcttga tcctgggggc caaactccac cccacgctga
                      221                                                                                 290

                      1051                                                                                1120
TRPV1 (NM_031982)     agctggaaga gatcaccaac aggaaggggc tcacgccact ggctctggct gctagcagtg ggaagatcgg

TRPV1_SON (LC008303) agctggaaga gatcaccaac aggaaggggc tcacgccact ggctctggct gctagcagtg ggaagatcgg
                      291                                                                                 360

                      1121                                                                                1190
TRPV1 (NM_031982)     ggtcttggcc tacattctcc agagggagat ccatgaaccc gagtgccgac acctatccag gaagttcacc
                                                                                  ex07F
TRPV1_SON (LC008303) ggtcttggcc tacattctcc agagggagat ccatgaaccc gagtgccgac acctatccag gaagttcacc
                      361                                                 ex07F                           430

                      1191                                                                                1260
TRPV1 (NM_031982)     gaatgggcct atgggccagt gcactcctcc ctttatgacc tgtcctgcat tgacacctgt gaaaagaact

TRPV1_SON (LC008303) gaatgggcct atgggccagt gcactcctcc ctttatgacc tgtcctgcat tgacacctgt gaaaagaact
                      431                                                                                 500

                      1261                                                                                1330
TRPV1 (NM_031982)     cggttctgga ggtgatcgct tacagcagca gtgagacccc taaccgtcat gacatgcttc tcgtggaacc

TRPV1_SON (LC008303) cggttctgga ggtgatcgct tacagcagca gtgagacccc taaccgtcat gacatgcttc tcgtggaacc
                      501                                                                                 570

                      1331                                                                                1400
TRPV1 (NM_031982)     cttgaaccga ctcctacagg acaagtggga cagatttgtc aagcgcatct tctacttcaa cttcttcgtc

TRPV1_SON (LC008303) cttgaaccga ctcctacagg acaagtggga cagatttgtc aagcgcatct tctacttcaa cttcttcgtt
                      571                                ex08R                                            640

                      1401                                                                                1470
TRPV1 (NM_031982)     tactgcttgt atatgatcat cttcaccgcg gctgcctact atcggcctgt ggaaggcttg ccccccctata

TRPV1_SON (LC008303) tactgcttgt atatgatcat cttcaccgcg gctgcctact atcggcctgt ggaaggcttg ccccccctata
                      641                                                                                 710

                      1471                                                                                1540
TRPV1 (NM_031982)     agctgaaaaa caccgttggg gactatttcc gagtcaccgg agagatcttg tctgtgtcag gaggagtcta

TRPV1_SON (LC008303) agctgaaaaa caccgttggg gactatttcc gagtcaccgg agagatcttg tctgtgtcag gaggagtcta
                      711                                                                                 780
```

```
                      1541                                                                                1610
TRPV1 (NM_031982)     cttcttcttc cgagggattc aatatttcct gcagaggcga ccatccctca agagtttgtt tgtggacagc

TRPV1_SON (LC008303) cttcttcttc cgagggattc aatatttcct gcagaggcga ccatccctca agagtttgtt tgtggacagc
                      781                                                                                 850

                      1611                                                                                1680
TRPV1 (NM_031982)     tacagtgaga tacttttctt tgtacagtcg ctgttcatgc tggtgtctgt ggtactgtac ttcagccaac

TRPV1_SON (LC008303) tacagtgaga tacttttctt tgtacagtcg ctgttcatgc tggtgtctgt ggtactgtac ttcagccaac
                      851                                                                                 920

                      1681                                                                                1750
TRPV1 (NM_031982)     gcaaggagta tgtggcttcc atggtgttct ccctggccat gggctggacc aacatgctct actatacccg
                                           ex11F
TRPV1_SON (LC008303) gcaaggagta tgtggcttcc atggtgttct ccctggccat gggctggacc aacatgctct actatacccg
                      921                  ex11F                                                          990

                      1751                                                                                1820
TRPV1 (NM_031982)     aggattccag cagatgggca tctatgctgt catgattgag aagatgatcc tcagagacct gtgccggttt

TRPV1_SON (LC008303) aggattccag cagatgggca tctatgctgt catgattgag aagatgatcc tcagagacct gtgccggttt
                      991                                                                                 1060

                      1821                                                                                1890
TRPV1 (NM_031982)     atgttcgtct acctcgtgtt cttgtttgga ttttccacag ctgtggtgac actgattgag gatgggaaga

TRPV1_SON (LC008303) atgttcgtct acctcgtgtt cttgtttgga ttttccacag ctgtggtgac actgattgag gatgggaaga
                      1061                                                                                1130

                      1891                                                                                1960
TRPV1 (NM_031982)     ataactctct gcctatggag tccacaccac acaagtgccg ggggtctgcc tgcaagccag gtaactctta

TRPV1_SON (LC008303) ataactctct gcctatggag tccacaccac acaagtgccg ggggtctgcc tgcaagccag gtaactctta
                      1131                                                                                1200

                      1961                                                                                2030
TRPV1 (NM_031982)     caacagcctg tattccacat gtctggagct gttcaagttc accatcggca tgggcgacct ggagttcact

TRPV1_SON (LC008303) caacagcctg tattccacat gtctggagct gttcaagttc accatcggca tgggcgacct ggagttcact
                      1201                                                                                1270

                      2031                                                                                2100
TRPV1 (NM_031982)     gagaactacg acttcaaggc tgtcttcatc atcctgttac tggcctatgt gattctcacc tacatccttc

TRPV1_SON (LC008303) gagaactacg acttcaaggc tgtcttcatc atcctgttac tggcctatgt gattctcacc tacatccttc
                      1271                                                                                1340

                      2101                                                                                2170
TRPV1 (NM_031982)     tgctcaacat gctcattgct ctcatgggtg agaccgtcaa caagattgca caagagagca agaacatctg
                                                                                          ex13F
TRPV1_SON (LC008303) tgctcaacat gctcattgct ctcatgggtg agaccgtcaa caagattgca caagagagca agaacatctg
                      1341                                                                 ex13F  1410

                      2171                                                                                2240
TRPV1 (NM_031982)     gaagctgcag agagccatca ccatcctgga tacagagaag agcttcctga agtgcatgag gaaggccttc

TRPV1_SON (LC008303) gaagctgcag agagccatca ccatcctgga tacagagaag agcttcctga agtgcatgag gaaggccttc
                      1411                                                                                1480

                      2241                                                                                2310
TRPV1 (NM_031982)     cgctctggca agctgctgca ggtggggttc actcctgacg gcaaggatga ctaccggtgg tgtttcaggg

TRPV1_SON (LC008303) cgctctggca agctgctgca ggtggggttc actcctgacg gcaaggatga ctaccggtgg tgtttcaggg
                      1481                                                                                1550
```

Fig. 2. Nucleotide sequences of mRNAs of full-length TRPV1 and TRPV_SON.

The whole nucleotide sequences for mRNAs of TRPV1 and TRPV1_SON that are registered to NCBI database are shown. Underlined nucleotides correspond to primer recognition sites used in this study. Nucleotides shown in squares are exon gaps. The start and stop codons are shown in red.

Co-localization of TRPV1 with AVP/OT

In order to identify whether TRPV1 is expressed by AVP neurons or OT neurons at the protein level, immunofluorescence staining was performed (Fig. 3). Fluorescence signals of Alexa 488 and 633 are presented in green and red, respectively. Green (Alexa 488) signals observed in the upper two images correspond to AVP- and OT-like immunoreactivity. Neurons showing AVP-like immunoreactivity (arrow heads) are found in the ventral side of the SON, whereas neurons showing OT-like immunoreactivity (arrows) are found in the dorsal region. Red (Alexa 633) signals shown in the middle two images represent TRPV1-like immunoreactivity. Merged images are presented at the bottom. TRPV1-like immunoreactivity is found solely in the neurons showing AVP-like immunoreactivity (arrow heads); but not OT-like immunoreactivity. In some neurons showing OT-like immunoreactivity, nuclei were stained with TRPV1, however, no yellow signal was found in OT neurons. The strong red and green signals present at the bottom left part of the images in the left column are likely to be the autofluorescence of red blood cells.

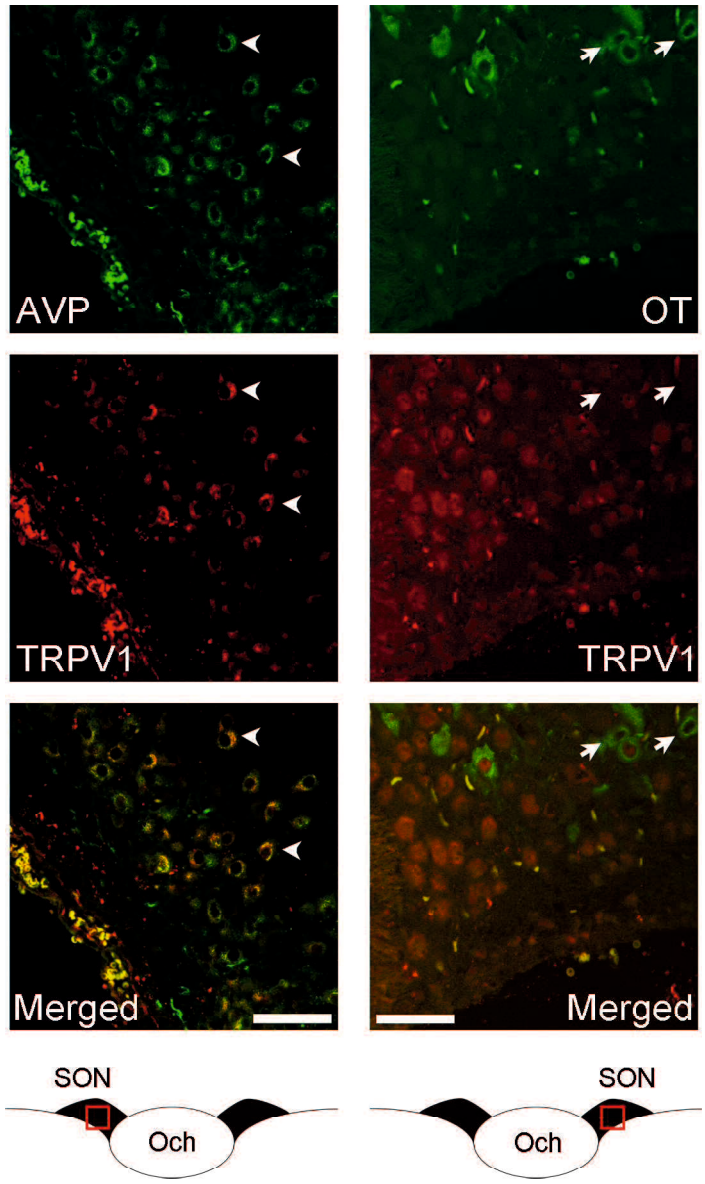

Fig. 3. Immunohistochemistry for TRPV1 and AVP in the SON.

Signals of Alexa 488 (upper) and Alexa 633 (middle) are pictured in the pseudocolors, green and red. The green signals observed in the upper left and right images indicate the AVP-like and OT-like immunoreactivity, respectively. The arrowheads and arrows point out AVP-positive and OT-positive neurons, respectively. The red signals observed in the middle two images indicate TRPV1-like immunoreactivity. The bottom two images are the merged images of those in the upper two lines of the images. Scale bars 50 μm. The locations of the areas, from which the fluorescence images are captured, are shown in the illustration at the bottom. Och: optic chiasm.

Hyperosmolality-induced responses in rat SON neurons

The results mentioned above indicate that full-length TRPV1 molecule is expressed in AVP neurons in rats. We next sought the evidence for functional activity of this full-length TRPV1 channel, using whole-cell patch-clamp and $[Ca^{2+}]_i$ imaging techniques. It has been reported previously that mouse SON neurons do not respond to capsaicin, a TRPV1 agonist [80]. This result is consistent with the idea that the N-terminal portion of TRPV1 is missing in mice, considering that the N-terminal portion contains two crucial capsaicin-binding sites [35, 101]. Providing, however, that full-length TRPV1 is expressed in SON neurons, capsaicin should evoke cationic currents and $[Ca^{2+}]_i$ elevation in rat SON neurons. Capsaicin at 100 nM (n = 8) and 1 μM (n = 6) did not cause a detectable $[Ca^{2+}]_i$ increase in SON neurons that responded to the hyperosmolarity stimulus (exposure to 50 mM of mannitol) as well as to high K^+ with a marked increase in $[Ca^{2+}]_i$ (Fig. 4). Mannitol evoked reversible $[Ca^{2+}]_i$ increases in 14 out of 68 (20.6 %) SON neurons examined. The average amplitude of the mannitol-induced $[Ca^{2+}]_i$ increase was 158 ± 30 nM (n = 14). The mannitol-induced $[Ca^{2+}]_i$ increase was completely abolished when Ca^{2+} was omitted from the perfusion solution

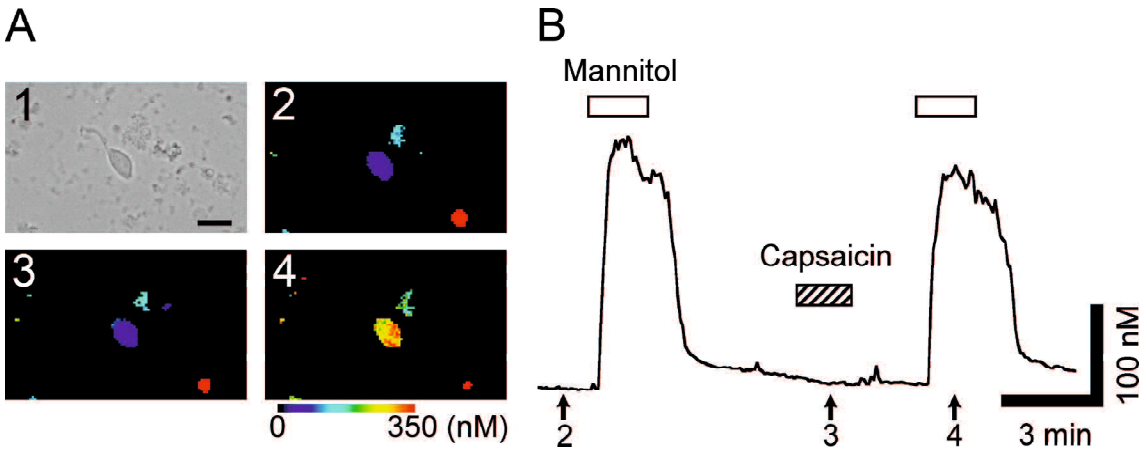

Fig. 4. Properties of $[Ca^{2+}]_i$ responses to mannitol in rat SON neurons.

(A) A bright field picture of a rat SON neuron (1) (scale bar 20 μm) and pseudocolor $[Ca^{2+}]_i$ images (2-4) obtained in resting condition (2), during 1 μM capsaicin application (3), and during 50 mM mannitol stimulation (4). (B) The time course of the response to mannitol obtained from the same cell. Horizontal bars in this and subsequent figures indicate the time at which drugs were added.

(n = 4). In contrast, $[Ca^{2+}]_i$ responses were not affected by the Na^+ channel blocker, TTX, at 1 μM: the peak of mannitol responses in the absence and presence of TTX was 185 ± 84 and 164 ± 61 nM, respectively (the ratio between the two responses was 121 ± 38%, P = 0.68, n = 4).

$[Ca^{2+}]_i$ responses in SON neurons isolated from transgenic rats

It has been demonstrated previously that TRPV1 is expressed in AVP neurons in rat SON [58]. In the present study, we have also found that the distribution of TRPV1 immunoreactivity was confined to the ventral region where most AVP-immunoreactive neurons dwell. In the next series of experiments, we examined whether the osmoreceptive responses are seen only in AVP neurons. In order to confirm these results, we used two transgenic rats, AVP-eGFP [92, 98] and OT-mRFP [19]. In 13 out of 17 AVP neurons that were identified by their GFP fluorescence $[Ca^{2+}]_i$ responses to mannitol (50 mM) were observed (Fig. 5). Conversely, none out of ten OT neurons that were identified by their RFP fluorescence responded to mannitol (50 mM) with $[Ca^{2+}]_i$ rise.

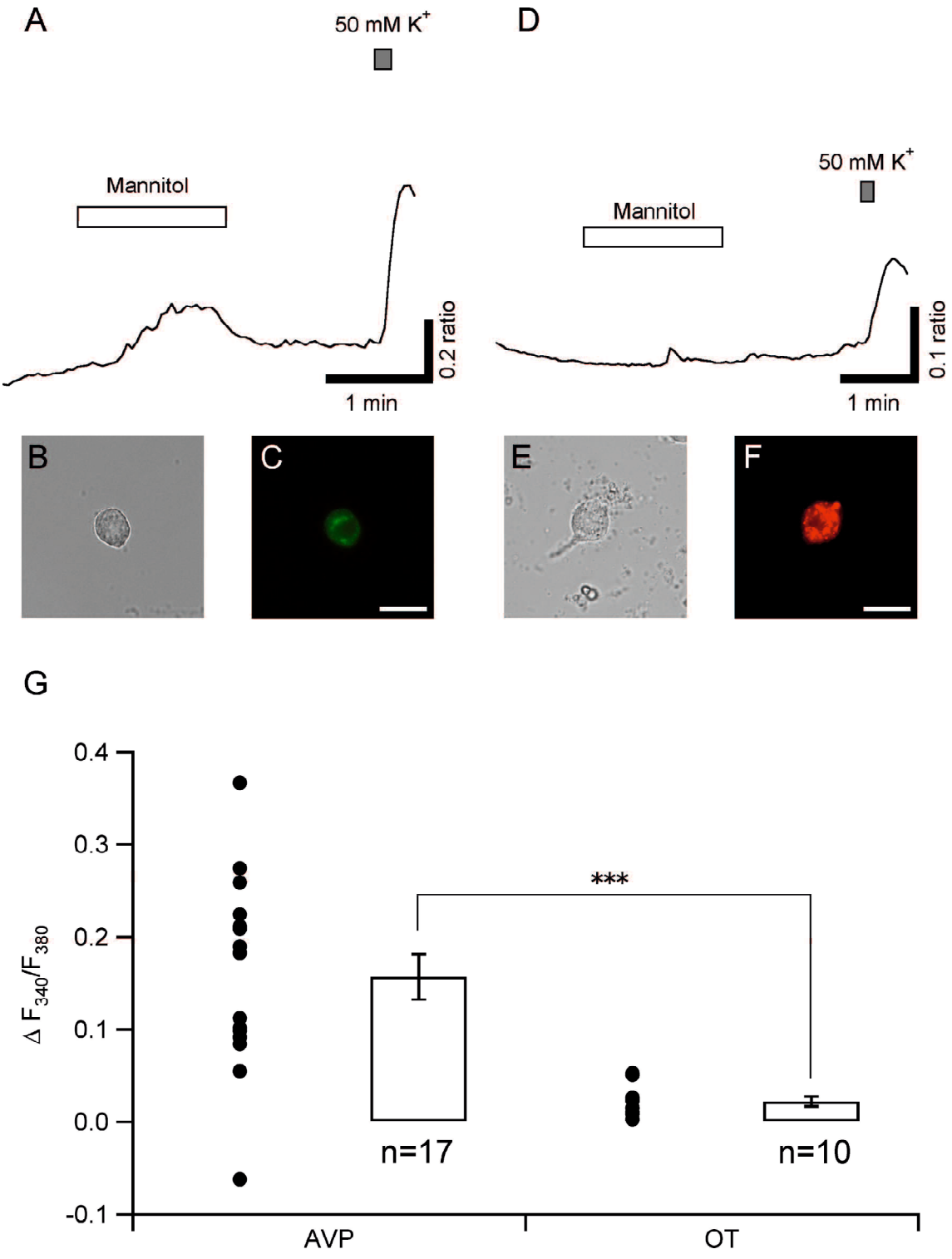
A
50 mM K+
Mannitol
0.2 ratio
1 min
D
50 mM K+
Mannitol
0.1 ratio
1 min
B
C
E
F
G
0.4
0.3
0.2
0.1
0.0
-0.1
Δ F340/F380
***
n=17
n=10
AVP
OT

Fig. 5. The $[Ca^{2+}]_i$ responses to mannitol observed in AVP and OT neurons identified by the GFP and RFP fluorescence.

(A) A representative *F340/F380* ratio response observed in the AVP neuron bright field image of which is shown (B) and GFP fluorescence image in (C); scale bar 25 μm. (D) A representative *F340/F380* ratio response observed in an OT neuron (E and F shows its bright field and RFP fluorescent images respectively). (G) Summary data for the ratio response obtained from identified AVP and OT neurons (n = 17 and 10, respectively). (***: $p<0.001$).

TRPV1-related drugs affect hyperosmolality-induced $[Ca^{2+}]_i$ responses

Subsequently, we examined whether the mannitol-induced responses in SON neurons are affected by TRPV1 antagonists in wild-type Wistar rats. The non-selective TRPV antagonist, ruthenium red (RR), and the two selective TRPV1 antagonists, capsazepine (CPZ) and BCTC, both administered at 10 μM, suppressed mannitol-induced increases of $[Ca^{2+}]_i$ by 92 ± 6.4 %, 99 ± 0.32 % and 81 ± 15 %, respectively, when compared to the control mannitol responses obtained in the absence of the TRPV antagonists (Fig. 6). At the same time, CPZ (10 μM) had little or no effect on high K^+ (50 mM)-evoked $[Ca^{2+}]_i$ responses: the high K^+ responses in the absence and presence of CPZ were 599 ± 85 and 577 ± 89 nM, respectively (the inhibition was at 2.3 ± 3.4 %, n = 11) (Fig. 7). Similarly, BTCT (10 μM) had only a small effect on high K^+-evoked $[Ca^{2+}]_i$ responses, the amplitudes of which in the absence and in the presence of BCTC were 785 ± 65 and 683 ± 76 nM, respectively (the inhibition was 13 ± 7.9 %, n = 12) (Fig. 8). These results indicate that the effects of CPZ and BCTC are selective for TRPV1 channels, and their effects on voltage-dependent Ca^{2+} channels are negligible.

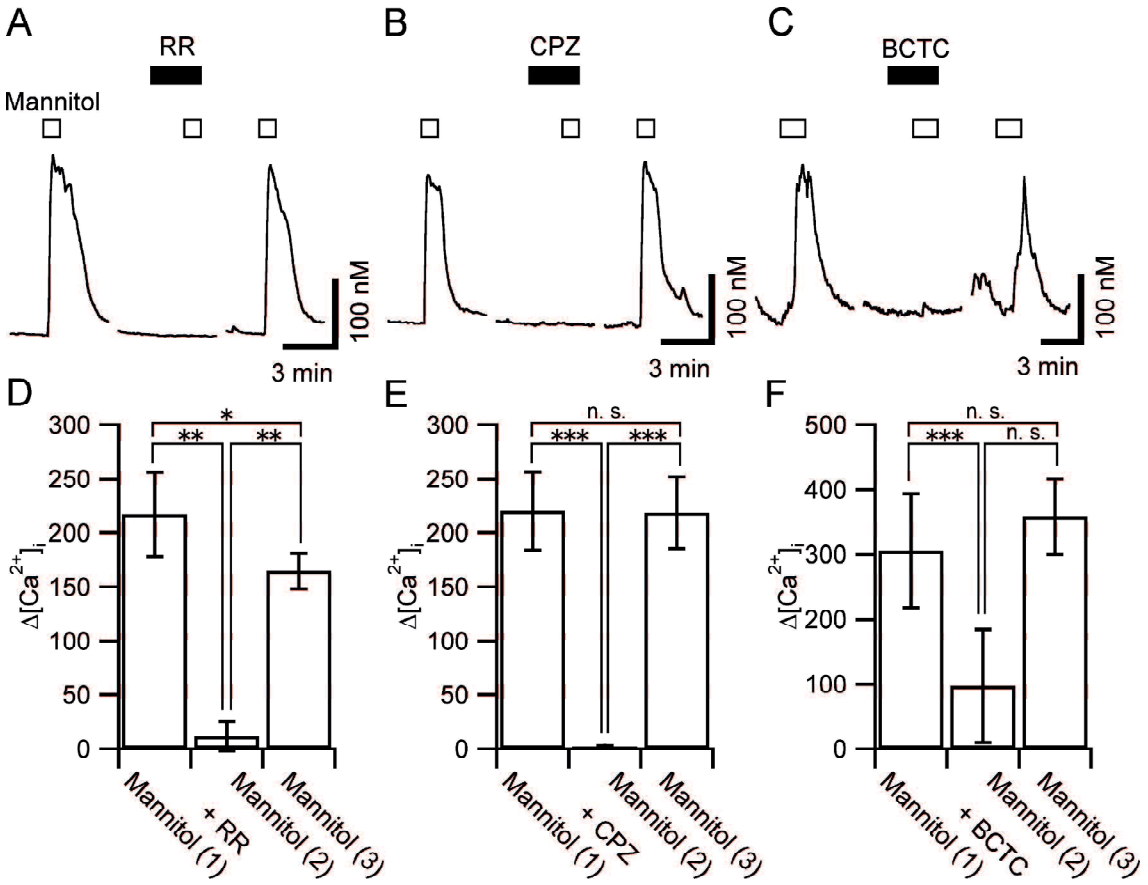

Fig. 6. $[Ca^{2+}]_i$ responses to mannitol and their inhibition by TRPV1 antagonists in SON neurons.

(A-C) Representative $[Ca^{2+}]_i$ responses to mannitol (50 mM) in control conditions and in the presence of TRPV1 antagonists, ruthenium red (RR), capsazepine (CPZ) and N-(4-tertiarybutylphenyl)-4-(3-cholorphyridin-2-yl)tetrahydropyrazine-1(2H)-carbox-amide (BCTC). The interruptions in the traces are 2-20 min. (D-F) Summary data for the $[Ca^{2+}]_i$ responses (the $[Ca^{2+}]_i$ was calculated by subtracting the basal $[Ca^{2+}]_i$ level from the peak of $[Ca^{2+}]_i$ response) in control before, in the presence of RR (n = 10), CPZ (n = 9) or BCTC (n = 4), and after wash-out. (*: $p<0.05$, **: $p<0.01$, ***: $p<0.001$).

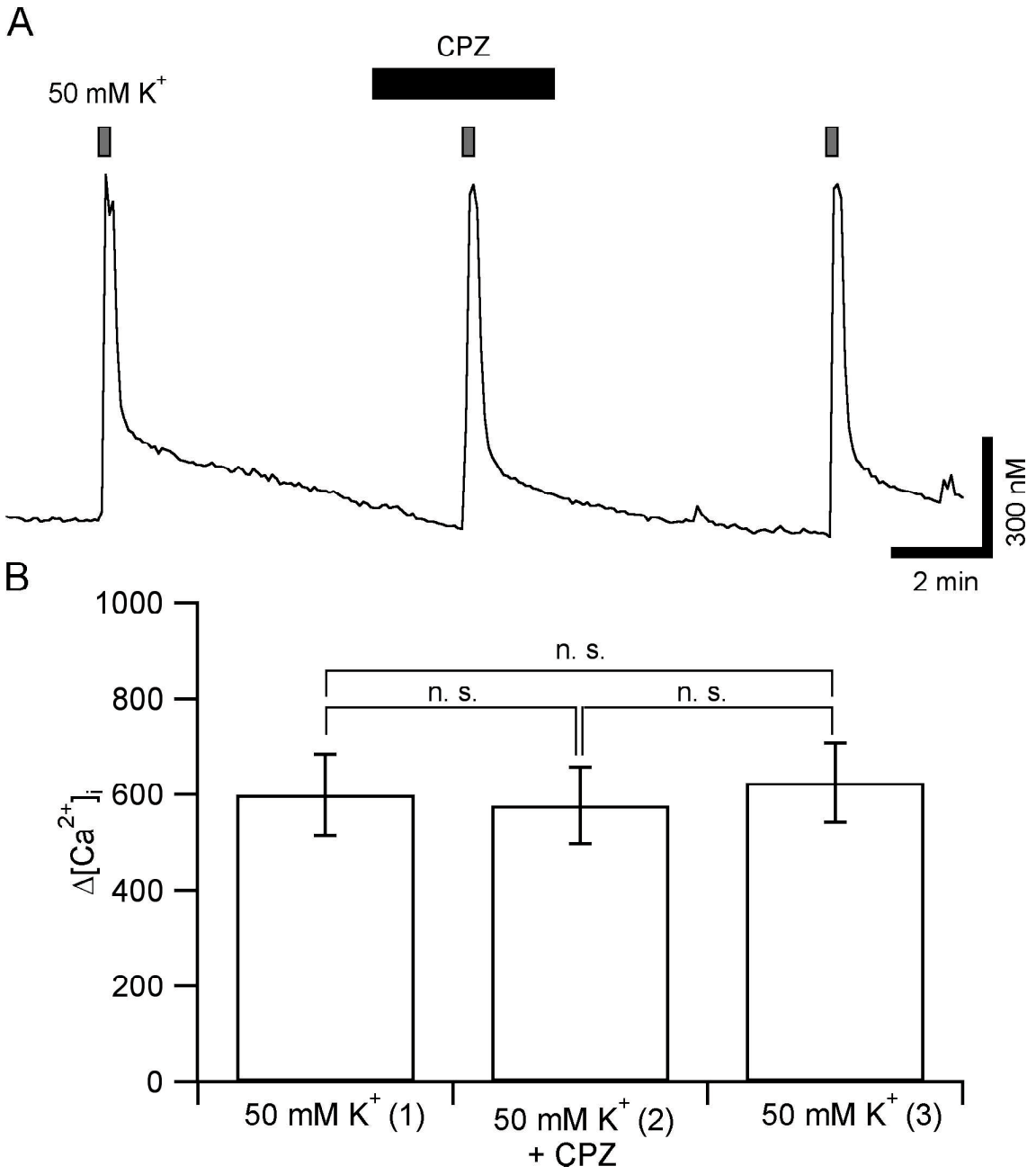

Fig. 7. Effects of TRPV1 antagonist, capsazepine, on 50 mM K^+-induced $[Ca^{2+}]_i$ increases in rat SON neurons.

(A) Representative $[Ca^{2+}]_i$ responses to 50 mM K^+ in control conditions and in the presence of TRPV1 antagonists, capsazepine (CPZ). (B) Summary data for the $[Ca^{2+}]_i$ responses (the $[Ca^{2+}]_i$ was calculated by subtracting the basal $[Ca^{2+}]_i$ level from the peak of $[Ca^{2+}]_i$ response) in control before, in the presence of CPZ (n = 11) and after wash-out. (*: $p<0.05$, **: $p<0.01$, ***: $p<0.001$).

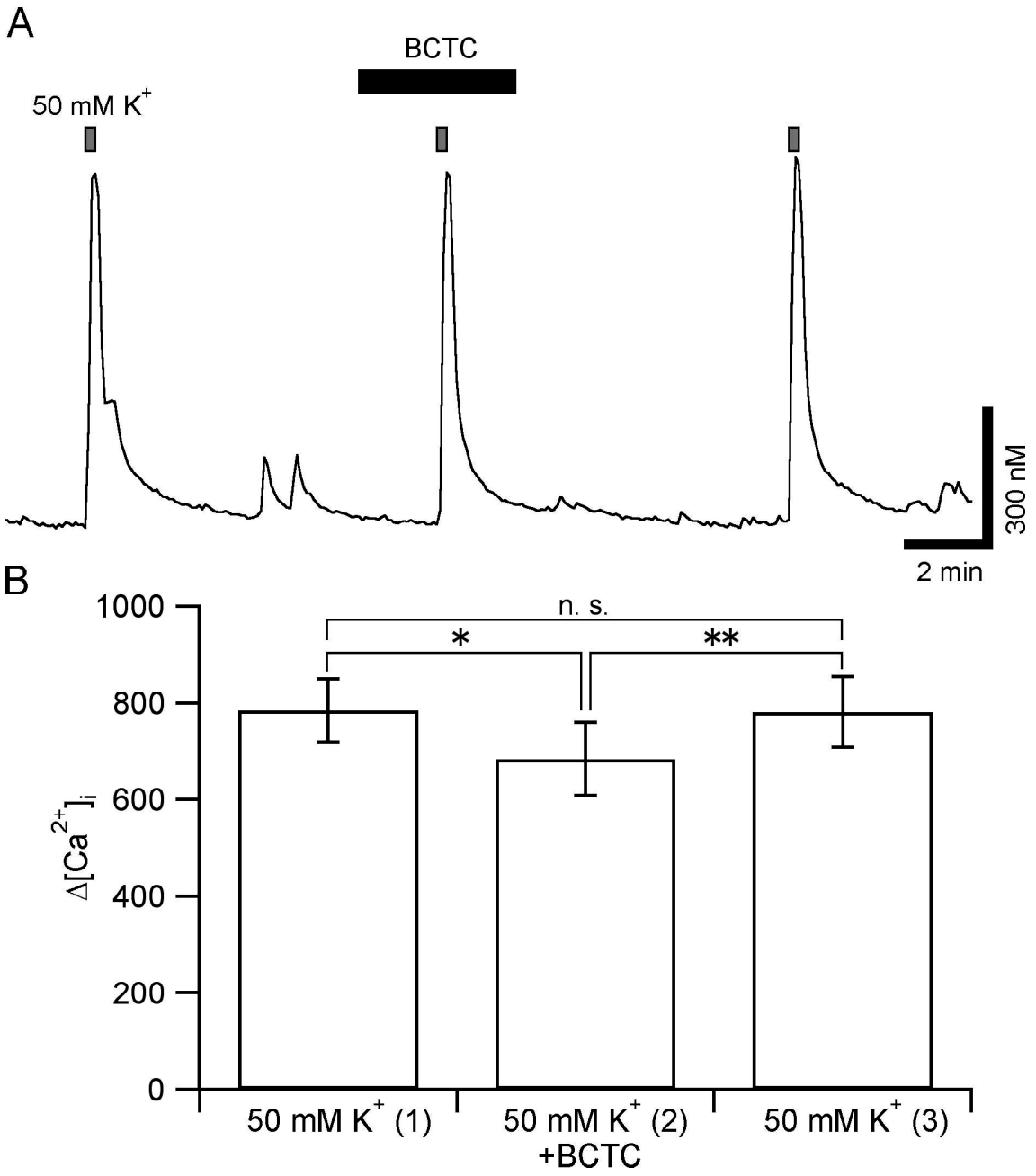

Fig. 8. Effects of TRPV1 antagonist, N-(4-tertiarybutylphenyl)-4-(3-cholorphyridin-2-yl)tetrahydropyrazine-1(2H)-carbox-amide, on 50 mM K^+-induced $[Ca^{2+}]_i$ increases in rat SON neurons.

(A) Representative $[Ca^{2+}]_i$ responses to 50 mM K^+ in control conditions and in the presence of TRPV1 antagonists, N-(4-tertiarybutylphenyl)-4-(3-cholorphyridin-2-yl)tetrahydropyrazine-1(2H)-carbox-amide (BCTC). (B) Summary data for the $[Ca^{2+}]_i$ responses (the $[Ca^{2+}]_i$ was calculated by subtracting the basal $[Ca^{2+}]_i$ level from the peak of $[Ca^{2+}]_i$ response) in control before, in the presence of BCTC (n = 12) and after wash-out. (*: $p<0.05$, **: $p<0.01$, ***: $p<0.001$).

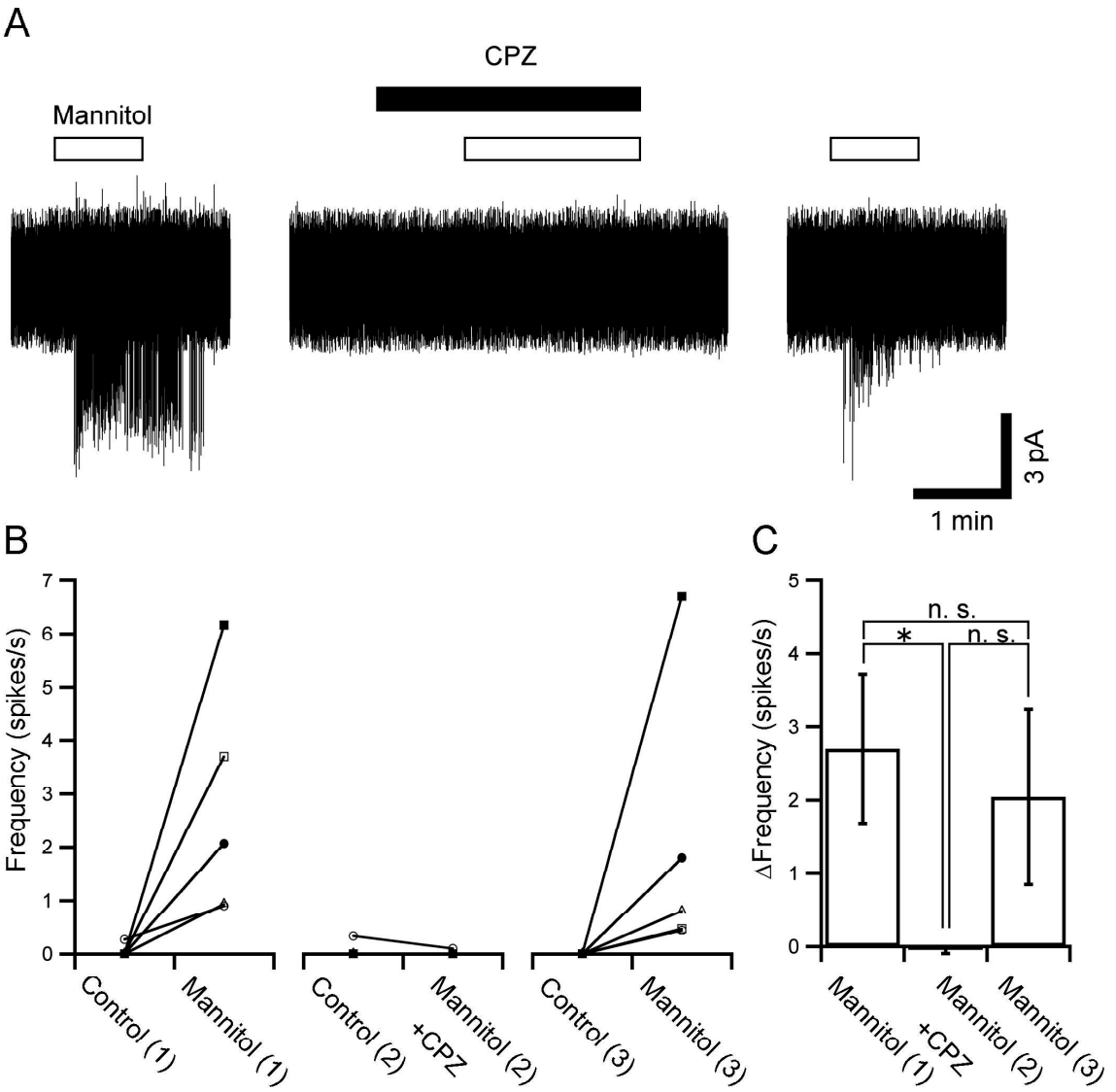

Fig. 9. Effects of TRPV1 antagonist, capsazepine, on mannitol-induced increases in the firing rate in rat SON neurons.

(A) Representative traces of the action potential discharges induced by mannitol (50 mM) and their block by 10 μM capsazepine (CPZ) obtained from a single SON neuron. The interruptions in the trace are 3-5 min. The electrical activity was monitored in the on-cell configuration of the patch-clamp technique (holding potential: -60 mV). (B) Changes in the firing frequency measured before and during mannitol application in 5 SON neurons and effect of 10 μM CPZ. (C) Summary data for the firing rate in response to mannitol in control, in the presence of CPZ and after wash-out (n = 5). (*: $p<0.05$).

Finally, in all five SON neurons CPZ (10 mM) reversibly suppressed an increase in the action potential frequency induced by 50 mM mannitol (n = 5, Fig. 9).

Temperature-dependence of capsaicin-induced responses in rat SON neurons

Although the sensitivity of mannitol-induced action potential firing rate and $[Ca^{2+}]_i$ to specific antagonists suggests the role for full-length TRPV1, the absence of response to capsaicin remains surprising, because the full-length TRPV1 possesses all 36 amino acids that are important for the action of capsaicin [101]. It has been demonstrated, however, that hyperosmolality-induced $[Ca^{2+}]_i$ transients in HEK293 cells show strong temperature-dependence [59]. As shown in Figs. 10 and 11, SON neurons, that were insensitive to capsaicin at 24 ºC, generated *bona fide* $[Ca^{2+}]_i$ transients at 36 ºC. In the voltage-clamp mode (Figs. 10A, B), capsaicin (100 nM) did not induce detectable currents at 24 ºC, whereas at 36 ºC, capsaicin (100 nM) induced inward currents at the holding potential of -60 mV (n = 4). The amplitude of the peak inward currents was -41.2 ± 18.7 pA. A characteristic I-V relation of the capsaicin-induced currents recorded at 36 ºC is shown in Fig. 10D. The reversal potential (E_{rev}) of the capsaicin-evoked currents was estimated at -46.4 ± 4.1 mV (n = 4), which is close to the E_{rev} of SIC current in

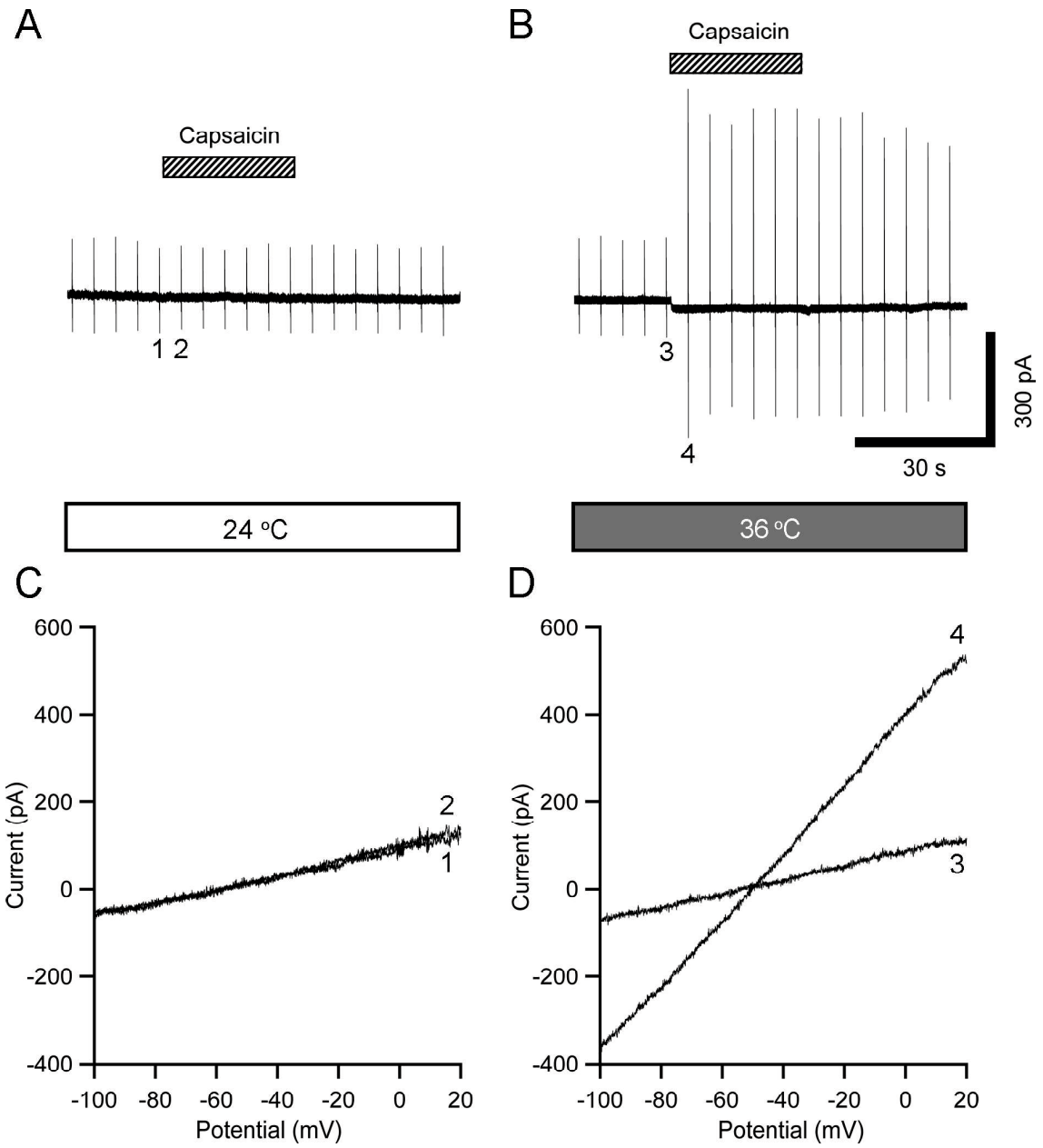

Fig. 10. Temperature dependence of capsaicin induced currents.

(A and B) Representative time courses for membrane currents induced by capsaicin (0.1 μM) at 24 and 36 °C. (C and D) I-V relations of currents in response to a ramp voltage ramps (-100 to 20 mV, in 100 ms) before and during capsaicin application obtained at 24 and 36 ºC. The I-V relations in (C) and (D) were obtained during the two ramp commands indicated by 1 and 2 in (A), 3 and 4 in (B), respectively.

rat SON [62]. Similarly, capsaicin (100 nM) caused only a minute $[Ca^{2+}]_i$ increase (8.5 ± 2.7 nM) in nine SON neurons that responded to mannitol (50 mM) with a large $[Ca^{2+}]_i$ transients (135 ± 15 nM) at 24°C. In contrast, in the same neurons, capsaicin (100 nM) evoked significant $[Ca^{2+}]_i$ elevations (134 ± 14 nM) at 36 ºC (Fig. 11) in all nine SON neurons that responded to mannitol (50 mM). These $[Ca^{2+}]_i$ responses to capsaicin (100 nM) observed at 36 ºC were reversibly suppressed (by 97 ± 2.3 %) by CPZ (10 μM) in seven SON neurons (Fig. 12). The amplitude of $[Ca^{2+}]_i$ increases to mannitol also tended to increase by at higher temperatures, but without significant difference. At the same time, all 53 SON neurons that did not respond to mannitol (50 mM) showed no response to capsaicin (100 nM) at 36 ºC. In 20 out of these 53 SON neurons, no $[Ca^{2+}]_i$ response was observed even when capsaicin concentration was increased to 1 μM.

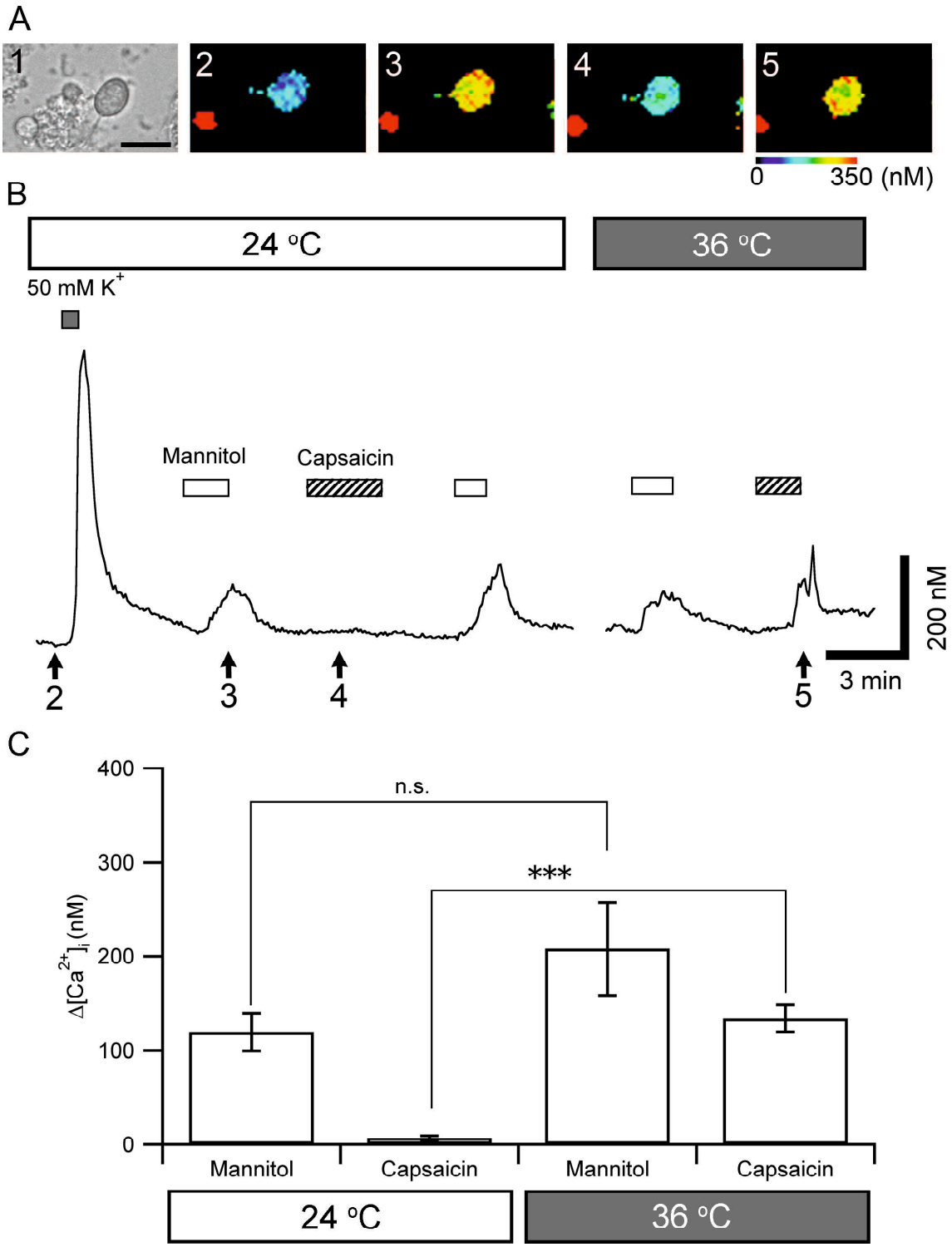
A
1
2
3
4
5
0
350 (nM)
B
24 °C
36 °C
50 mM K+
Mannitol
Capsaicin
200 nM
3 min
2
3
4
5
C
400
300
200
100
0
Δ[Ca2+]i (nM)
n.s.
***
Mannitol
Capsaicin
Mannitol
Capsaicin
24 °C
36 °C

Fig. 11. $[Ca^{2+}]_i$ responses to mannitol and capsaicin observed at 24 and 36 ºC.

(A) A bright field picture of a rat SON neuron (1) (scale bar 20 μm) and pseudocolor $[Ca^{2+}]_i$ images (2-4) obtained in resting condition (2), during 50 mM mannitol stimulation (3), during 100 nM capsaicin application at 24 ºC (4) and 36 ºC (5). (B) The $[Ca^{2+}]_i$ dynamic in response to mannitol and capsaicin obtained in the cell shown in (A). Note that the neuron not responding to capsaicin at 24 ºC responded to the same concentration of capsaicin when the temperature was increased to 36 ºC. (C) Summary data for the $[Ca^{2+}]_i$ responses induced by mannitol and capsaicin at 24 and 36 ºC (n = 9). (***: $p<0.001$).

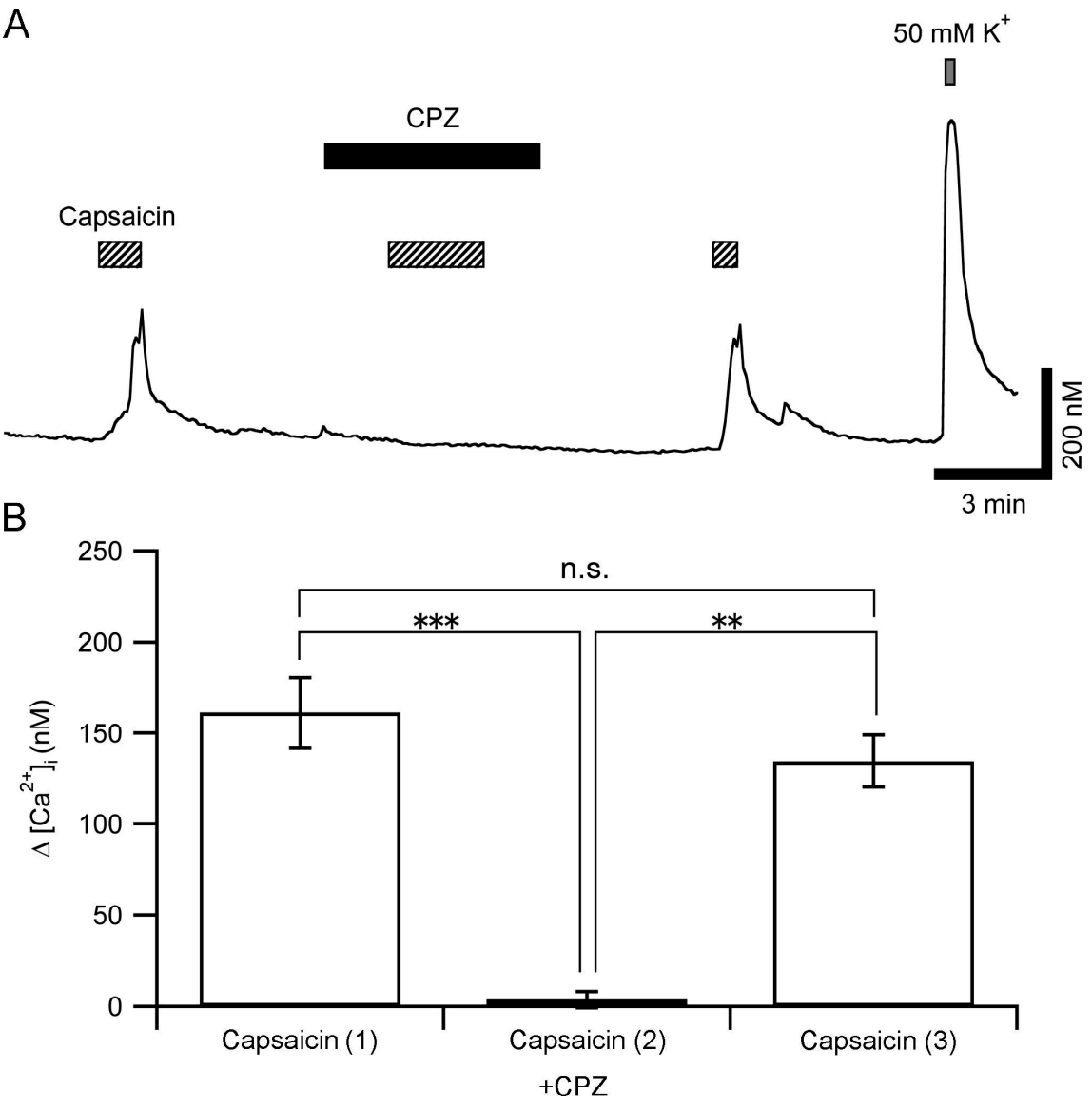

Fig. 12. $[Ca^{2+}]_i$ responses to capsaicin and their inhibition by capsazepine at 36 ºC.
(A) A representative time course for $[Ca^{2+}]_i$ responses to capsaicin (100 nM) and the block of the response by 10 μM CPZ observed at 36 ºC. (B) Summary data for the $[Ca^{2+}]_i$ responses induced by capsaicin and their block by CPZ at 36 ºC (n = 7). (**: $p<0.01$, ***: $p<0.001$).

DISCUSSION

Molecular types of TRPV1 detected in rat SON

The present study demonstrated that full-length *Trpv1* are expressed and are functional in rat SON neurons. We have detected two major bands (Figs. 1A and 1B) by RT-PCR associated with *Trpv1*-related variants: one corresponding to full length *Trpv1* and another having similar nucleotide length as the stretch-inhibitable nonselective cation channel found in the kidney [86]. We also confirmed that full-length *Trpv1* is expressed in SON using the primer pairs corresponding to the 5'- and 3'-terminal ends of the full-length *Trpv1* coding region. We detected two distinct sequences: one sequence of PCR products was identical to that of full-length *Trpv1* (NM 031982) and the other had the three nucleotide substitution, suggesting the existence of polymorphism of this gene between the strains of rats. The substitutions of G134T and C367A cause amino acid substitutions of Glu to Asp at position 18 and Pro to Gln at position 96, respectively, whereas the substation of C1400T is a none-sense substitution. These amino acid substitutions may not affect functions of TRPV1, because the former two amino acids are acidic, and for the latter, both the amino acids are neutral. Moreover, neither amino acid belongs to the reported site of capsaicin binding or phosphorylation by protein kinases. Furthermore, the

entire sequence was identical between cDNAs of the SON and DRG, indicating that the differences are not tissue, but rather strain specific.

The RT-PCR and sequencing results supporting the presence of full-length *Trpv1* in rat SON were further corroborated by the immunohistochemical staining of the SON with the antibody directed against the N-terminal portion of TRPV1. The TRPV1 immunolabeling was detected in the neurons with AVP-like immunoreactivity in the ventral part of the SON, but not in the neurons with OT-like immunoreactivity in the dorsal part of the SON, suggesting that TRPV1 N-terminal is exclusively expressed in AVP neurons. The TRPV1 immunoreactivity was also found inside the nucleus of some OT neurons, for which we do not have an explanation, although we may suggest that nuclear proteins do not function as ion channels in these neurons.

When analysing cDNA sequence of the other major PCR band (Fig. 1B), which seemingly corresponds to the *stretch-inhibitable nonselective cation channels* cloned from rat kidney [86], we found a new N-terminal splice varitant, *Trpv1_SON* (NCBI Accession No. LC008303). There have been three N-terminal splice variants of *Trpv1* reported to date, and *Trpv1_SON* does not match any of them. TPRV1_SON has a similarity to VR.5'sv in the amino acid sequences, but retains the 60 amino acids in exon 7 region that

VR.5'sv lacks. This molecule may play a pivotal role in SON neurons, since the intensity of the band was similar to that of full-length TRPV1. Furthermore we detected the same molecule in the DRG and hence we can even speculate that TRPV1_SON may contribute to pain sensation.

Responses to hyperosmolality and TRPV1-related drugs

The HEK-293 cells expressing full-length rat TRPV1 responded to mannitol-induced hyperosmolality with $[Ca^{2+}]_i$ increases [59]. Similarly 20 % of rat SON neurons responded to mannitol with a large increase in $[Ca^{2+}]_i$. This $[Ca^{2+}]_i$ response originates from Ca^{2+} entry, because it was completely abolished in a Ca^{2+}-free extracellular solution. Although mannitol activated action potential discharges in the on-cell recordings, the lack of effect of TTX on the mannitol-induced $[Ca^{2+}]_i$ response suggests that Ca^{2+} entry is independent of action potentials and may be mediated by SIC channels with high Ca^{2+} permeability [104]. Virtually complete block of the mannitol-induced $[Ca^{2+}]_i$ response by selective TRPV1 antagonists, CPZ and BCTC, indicates that hyperosmolality activates TRPV1, which results in cell depolarization and Ca^{2+} entry through TRPV1 channels themselves and voltage-dependent Ca^{2+} channels.

The TRPV1 agonist, capsaicin, added at 36 ºC, consistently evoked $[Ca^{2+}]_i$ increases in rat SON neurons that were sensitive to mannitol. Although the precise mechanism by which the temperature modulates the capsaicin efficacy remains unknown, it is likely to reflect a selective activation of TRPV1, because capsaicin did not affect $[Ca^{2+}]_i$ in 53 SON neurons insensitive to mannitol at 36 ^{o}C. The capsaicin-induced responses were reversibly blocked by the selective TRPV1 antagonist, CPZ, indicating that only those SON neurons which express TPRV1 respond to an increase in osmolality. Of note, it has been reported that the arginines in the N-terminal portion (at the 114 and 115 position) of TRPV1 are crucial for capsaicin binding and channel activation [35, 101]. Therefore, capsaicin-sensitivity of osmosensitive SON neurons provides another piece of supportive evidence that the TRPV1 molecule in the SON has the N-terminal portion.

Our findings differ from the results obtained in mouse SON neurons, in which electrophysiological responses to hyperosmolality were not blocked by CPZ and capsaicin was without any effect [80]. Distinct TRPV1 pharmacology may reflect a difference in TRPV1 molecules expressed in the SON of these two species, which difference may reflect the presence of the N-terminal portion in rats and its absence in mice.

Specific expression of TRPV1 in AVP neurons

Our immunohistochemical results indicate that TRPV1 with the N-terminal portion is co-expressed with AVP. This is in good agreement with the previous data that *Trpv1-4* mRNAs were detected in rat SON neurons that were laser-captured using an anti-AVP antibody [58]. These results are also consistent with our experiments on SON neurons isolated from transgenic rats that revealed that the mannitol response was observed solely in AVP but not in OT neurons. On the other hand, it has been reported that hyperosmotic stimuli resulted in excitation of OT neurons that were identified by milk-ejection-reflex and also in increased plasma OT levels in anesthetized rats [8], and that hypertonic (+ 60 mosmol/kg) challenge increased the firing frequency of immunohistochemically identified OT neurons in slice preparations of rat [21]. These results nonetheless do not contradict our present results, because there are several lines of evidence indicating that osmotic stimuli can excite OT neurons via multiple indirect mechanisms: neurons in the circumventricular organs such as OVLT and SFO can sense changes in the ECF osmolality and send excitatory synaptic inputs to the SON [72], astrocytes in the SON can mediate osmosensory signals to neighboring SON neurons [20], and hyperosmolality can increase miniature EPSCs in glutamatergic terminals innervating rat SON neurons [103]. Our

present results do not rule out, however, the presence of direct mechanisms that can excite OT neurons, since in the present study we have tested 50 mM mannitol stimulation, which increases the extracellular osmolality by only 30 mosmol/kg. Stronger osmotic stimuli might directly excite OT neurons possibly via molecules located in their plasma membrane.

Responses to mannitol were detected only in ~20 % of SON neurons, which is less than a half of all AVP neurons (these latter representing ~50% of neuronal cells in the SON). At the same time almost all AVP positive neurons also showed labelling for TRPV1. One possible explanation for the lack of mannitol responses in a subpopulation of AVP neurons could be that in some cells, the osmoreceptive response was too small to be detected, possibly because the response is tonically inhibited in our experimental conditions. It could also be, at least in part, due to little or no response from damaged AVP neurons following acute dissociation.

Molecular identity of the central osmoreceptor in rats

The molecular identity of the central osmoreceptor remains to be identified, however, a report on the lack of osmoreceptive responses in *Trpv1*-knock-out mice [80] suggests that

the osmoreceptor is composed by TRPV1-related molecules not only in mice, but also in other mammals. The results of our study indicate that rat SON neurons express full-length functional TRPV1 which are likely to be associated with osmosensing. First, SON neurons are sensitive to TRPV1-specific drugs, capsaicin, RR, CPZ and BCTC, similarly to DRG neurons or HEK-293 cells expressing full-length TRPV1. It appears that, at physiological temperatures near 36 ºC, rat SON neurons are pharmacologically indistinguishable from TRPV1-expressing cells, as long as TRPV1-related drugs are used. Second, the reversal potential of osmoreceptive currents in rat SON neurons is -42.3 ± 2.0 mV [62], which is close to the reversal potential of the capsaicin-induced currents measured in the present study. Third, both osmoreceptive SIC channels and TRPV1 channels have high permeability to Ca^{2+}. Fourth, both channels are activated and mediate Ca^{2+} entry in response to hyperosmolality. These results suggest that the cation channel that includes a full-length TRPV1, is a strong candidate for the osmoreceptor in rat SON neurons.

There are however significant differences between osmoreceptor and TRPV1 channel. The P_{Ca}/P_{Na} ratio of osmoreceptive channels in rat SON neurons is 5.3 [104] and that of HEK-293 cells expressing full-length TRPV1 is 9.6 [11]. The single channel conductance of SIC channels in rat SON neurons is 32 ± 2 pS [62], which is different from that of

capsaicin-activated channels in DRG neurons (46 ± 6 pS at -60 mV) [70]. The I-V relation of the capsaicin-induced currents observed in rat SON neurons in the present study is ohmic and the reversal potential was around -46 mV, which is almost identical to the I-V relation and reversal potential for osmoreceptive SIC currents recorded in rat SON neurons [62], but is different from I-V curves obtained in rat DRG neurons or in HEK293 cells and *Xenopus* oocytes expressing rat TRPV1; in which the current showed outward rectification and reversal at -30 to 0 mV [11, 60, 70, 71]. These differences suggest that the osmoreceptor in SON neurons may not be the TRPV1 homotetramer. It has been reported that TRPV1 assemble either as homotetramers or heterotetramers to form cation channels [22, 73] and that full-length TRPV1 and TRPV2 [73], and full-length TRPV1 and VR.5' [22] could co-assemble. It is possible that full-length TRPV1 composes heteromers with other members of TRPV family including the new N-terminal splice variant of TRPV1 found in the present study, TRPV1_SON, which may explain the above mentioned differences observed between rat SON neurons and the TRPV1-expressing cells. The functional differences could also be due to involvement of unidentified accessory proteins or intracellular signal transduction mechanisms that interact with TRPV1 channels and affect their function. The TRPV1 expression levels were considerably lower in SON

tissues than in DRG tissues could also explain the differences: a much lower level of TRPV1 expression in SON neurons might make cation channels of a different nature from those in DRG neurons. Further studies at molecular and cellular levels are needed to uncover the molecular identity of the central osmoreceptor in SON neurons.

CHAPTER 2

Vasopressin-induced intracellular Ca^{2+} concentration responses in non-neuronal cells of the rat dorsal root ganglion

INTRODUCTION

AVP secreted into systemic circulation has various physiological roles through the activation of its receptors. The action of AVP is mediated through a specific subtype of 7 transmembrane domains G-protein coupled receptors. The AVP receptors are represented by 3 distinct subtypes classified as V_{1a}, V_{1b} and V_2 receptors [54].

DRG contain the cell bodies of pseudounipolar neurons conveying and integrating somatic sensory inputs (pain, temperature, mechanosensation) from the periphery to the spinal cord. According to somata's diameters, one can distinguish 3 types of neurons: large, medium and small, corresponding to different conductivities and sensory modalities [78]. Obviously, the classification of DRG neurons is much more complex and is also based on the action potential configuration, the level of myelination and the expression of important molecular markers such as ion channels [45].

DRG neurons are surrounded by both satellite glial cells [27] and myelinating Schwann cells. Both types of the DRG glial cells are derived from neural crest [33, 44], and express S-100 protein [95] but have several differences in their functions and localization.

The satellite glial cells surround completely around the cell bodies of DRG neurons, and the distance between the two types of cells is about 20 nm [66]. Little is known about

the function of the satellite glial cells, but a recent study suggests that the satellite glial cell has a significant role in controlling the microenvironment in ganglia [61]. The satellite glial cells express the glutamate-aspartate transporter and glutamine synthetase [56] and may play an important role in maintaining glutamate homeostasis in the DRG [2]. Another investigation implies the relevance between the satellite glial cells and the pain sensing mechanisms [99]. Silencing of the inwardly rectifying potassium channels, which are expressed only in the satellite cells among DRG cells, results in appearance of both spontaneous and evoked pain and decreased tolerance to innocuous stimuli.

The major physiological role of Schwann cells is myelinating the axons of PNS neurons and thus facilitating the saltatory conduction. Schwann cells also contribute to the neuronal survival and nerve regeneration processes by providing neurotrophic factors [53]. After the denervation, Schwann cells produce many types of neurotrophic factors such as brain-derived neurotrophic factor, nerve growth factor (NGF), glial cell line–derived neurotrophic factor, which stimulate the axonal growth and support the neuronal survive [82].

As written in PREFACE, Kai-Kai and co-workers have identified AVP immunoreactivity in neurons of rat DRG [36]. Shortly after, a different group

characterized the accumulation of inositol phosphates by application of AVP at concentrations in the micromolar range in rat DRG [31], and this phenomenon was dependent on the V_1 AVP receptor subtype. Based on these studies, we could assume that: i) AVP is also present in the PNS especially in neurons of the DRG and ii) the inositol phosphate pathway is involved through receptors coupled to G_q proteins, suggesting the existence of AVP receptors in ganglia cells and the possibility for the peptides to induce the production of inositol 1,4,5-trisphosphate ($InsP_3$) responsible for the activation of Ca^{2+} release channels seated on the membrane of the endoplasmic reticulum. Within the huge family of 2nd messengers, Ca^{2+} is widely considered as the most ubiquitous and the control of Ca^{2+} homeostasis in cells is of major importance for the regulation of development, excitation, contraction, neurotransmitter release, aging and apoptosis [89]. Taking all these aspects into consideration, the aim of the present study is to investigate the AVP-induced Ca^{2+} signaling in the cultured cells of the rat DRG. Our results show that AVP induces consistently a clear Ca^{2+} signal involving an $InsP_3$-evoked release of Ca^{2+} from the intracellular stores.

MATERIALS AND METHODS

DRG cell isolation and culture

DRG cells were isolated from adult male Sprague-Dawley rats (7-12 weeks old), using the procedures reported previously [39, 40, 64]. Animals were sacrificed according to the guidelines of the ethical committee of Tottori University, Japan. The rats were killed by cervical dislocation under anesthesia by an intraperitoneal injection of pentobarbital (5 mg/kg bw). Ganglia were dissected from the entire length of the vertebral column. Axons extending from the ganglia were removed under a stereoscopic microscope. The ganglia were incubated in Ca^{2+}/Mg^{2+}-free phosphate-buffered saline (PBS) containing 300 U/ml collagenase type IV (Worthington Biochemical, Lakewood, NJ, USA), 0.12 μg/ml DNase I and 1 mg/ml BSA for 2 h at 37˚C and then rinsed with PBS to remove the enzymes. They were then incubated in PBS containing 0.25% trypsin (Life technologies, California, USA) and 1 mg/ml BSA for 15 min at 37˚C. After the enzymatic digestion, the cells were gently triturated with a silicon-coated Pasteur pipette and centrifuged at 1000 rpm for 5 min to remove the enzymes. The cells were suspended in DMEM (Life technologies) with glucose (4.5 g/l) and plated onto coverslips (11 mm in diameter) coated with 50 mg/ml poly-D-lysine. The cells were kept at 37˚C in a humidified atmosphere of 95% air and 5%

CO_2 until use. The DMEM was supplemented with 10% FBS (MP Biochemicals, Irvine, CA, USA), 100 U/ml penicillin (Life technologies), 100 μg/ml streptomycin (Life technologies) and 5 μM cytosine–β–D-arabinofuranoside. The culture medium was changed every 2 days. The $[Ca^{2+}]_i$ measurements were performed between the 5th and 11th day of culture.

$[Ca^{2+}]_i$ measurements

The $[Ca^{2+}]_i$ in cultured rat DRG cells was measured with Fura-2, a fluorescent Ca^{2+} indicator, according to the procedure reported previously [64]. The cultured cells were incubated in HEPES-buffered Normal Locke's solution (NL; in mM: 140 NaCl, 5 KCl, 2 $CaCl_2$, 1.2 $MgCl_2$, 10 glucose, 10 HEPES, pH was adjusted to 7.4 with Tris; the osmolarity was between 298-300 mOsmol/l) containing 2 μM Fura-2/AM (Merck, Whitehouse Station, NJ, USA) and 0.01% Pluronic acid F-127 (Life technologies) for 60 min at room temperature (22-24ºC) in the dark. After the incubation, the coverslip was mounted onto the recording chamber (RC-25F, Warner Instruments, Hamden, USA) which is fixed on the stage of an inverted fluorescence microscope (IX71, Olympus, Tokyo, Japan). The cells were continuously perfused with solutions containing various experimental drugs through

polypropylene tubes connected to a peristaltic pump (Minipuls 3, Gilson, Middleton, WI, USA) at a flow rate of 1.4 ml/min. In this system, the solution around the cells could be changed rapidly within a few seconds. The Fura-2 fluorescence signal was detected through a UV objective lens (UApo 20×3/340, Olympus), and the florescence image passing through a band-pass filter (500 ± 10 nm) was captured by a cooled CCD camera (ORCA-ER, Hamamatsu Photonics). All experiments were performed at room temperature (22-24ºC).

Data acquisition and analysis

Data acquisition was made according to the procedure reported previously [64]. Briefly, Fura-2 images were captured at a sampling frequency of 0.2 Hz using Aqua Cosmos software (Hamamatsu Photonics). The fluorescent intensity at the excitation wavelengths of 340 nm (F340) and 380 nm (F380) was determined by the analyzing software (Aqua Cosmos, Hamamatsu Photonics). The ratio of fluorescence for each pixel obtained with the excitation at 340 and 380 nm (F340/F380) was used to calculate $[Ca^{2+}]_i$. A calibration curve of $[Ca^{2+}]_i$ for F340/F380 was determined using a series of Ca^{2+}-buffered solutions (Life technologies). To estimate the $[Ca^{2+}]_i$ levels in individual cells, regions of interest

(ROIs) were chosen to include the soma of each DRG cell, and average values for $[Ca^{2+}]_i$ in pixels contained in each ROI were calculated. The amplitude of $[Ca^{2+}]_i$ responses was expressed as $D[Ca^{2+}]_i$, which was calculated by subtracting average $[Ca^{2+}]_i$ levels during 2 min before AVP application from peak $[Ca^{2+}]_i$ amplitudes detected during 5 min after the onset of AVP application. Changes in the calculated $[Ca^{2+}]_i$ were analyzed by IGOR Pro (Wavemetrics, Lake Oswego, OR, USA) and Excel (Microsoft, Redmond, WA, USA). Data are presented as the means ± SEM. The statistical significance was assessed by One-factor analysis of variance (ANOVA) or Student's *t*-test. Differences were considered statistically significant if $P < 0.05$.

Immunocytochemistry

After the $[Ca^{2+}]_i$ measurements, the cells on some coverslips were analyzed for fluorescent immunocytochemistry to distinguish glial cells from other types of cells. All staining processes were made in the recording chamber keeping the observation field of the $[Ca^{2+}]_i$ measurement. After the $[Ca^{2+}]_i$ measurement, cells on the coverslips were perfused with PBS for 5 min and then fixed with PBS containing 4% paraformaldehyde (PFA) for 15 min. After the fixation, the cells were perfused with PBS for 5 min to remove PFA and

then permeabilized with PBS containing 0.1% Triton X-100 for 5 min. They were then perfused with PBS for 5 min and perfused with the blocking solution that consisted of PBS containing 10% donkey serum for 30 min. After the blocking, the cells were probed by the rabbit anti-bovine S-100 polyclonal antibody (dilution: 1:50; AbD Serotec, Kidlington, UK) for 12-15 h. Then the primary antibody was removed by perfusing the cells with PBS for 5 min. During this step, auto-fluorescence of the cells, those used for the $[Ca^{2+}]_i$ measurements, was captured by the CCD camera. Then, cells were probed with the secondary antibody, the donkey anti-rabbit IgG antibody (dilution: 1:300) conjugated with Alexa 488 (Life technologies). They were then mounted on the chamber to label anti-S-100 antibody for 1 h. Finally, the stained cells were perfused with PBS for 5 min, and fluorescence images of Alexa 488 were captured by the CCD camera.

In addition to the fluorescent immunocytochemistry, S-100-immunopositive cells were detected by the enzymatic immunocytochemistry, the procedures which have been reported previously [39]. In brief, after the blocking with 10% goat serum in PBS, the cells were probed by the anti-S100 antibody (dilution: 1:50; AbD Serotec) for 12-15 h. Then primary antibody was washed with PBS and cells were probed with the secondary antibody, HRP-conjugated goat anti-rabbit IgG antibody (dilution: 1:200) for 2 h. Finally, the probed

cells were visualized by 3,3'-Diaminobenzidine tetrahydrochloride (1 mg/ml) for 10 min and were counter stained with hematoxyline. All immunocytochemical experiments were performed at room temperature (22-24ºC).

RNA isolation and RT-PCR

Total RNAs used for reverse transcription-polymerase chain reaction (RT-PCR) were isolated from DRG tissues and cultured DRG cells using Trizol reagent (Life technologies) according to the manufacture's protocol. Reverse transcription was performed with 1 μg (DRG tissue) and 0.4 μg (cultured DRG cells) total RNA using PrimeScript RT-PCR Kit (Takara Bio Inc., Shiga, Japan) according to the manufacture's protocol. PCR was performed with 1μl of first-strand cDNA, a primer pair listed in Table 4 and Emerald Amp MAX PCR Master Mix (Takara Bio). The PCR profile was as follows: 94 ℃ for 30 seconds, 60 ℃ for 30 seconds, 72 ℃ for 30 seconds, for 30 cycles. After amplification, PCR products and 100 bp DNA ladder (New England Ipswich, MA, USA) were electrophoresed with TAE buffer on a 1.5% agarose gel (Bio-Rad laboratories, Inc., California, USA) containing 1 μg/ml ethidium bromide. Bands were excited by ultraviolet light and photographed.

Table 4. Primers for RT-PCR

Gene	Sequence	Product Size (bp)	Reference
V_{1a} receptor	GCGGAAAGACAGCGTCCTCGCGACA	416	[14]
	GCTCATGCTATCGGAGTCATCCTTGGCGAAT		
V_{1b} receptor	GTCAGCAGCATCAGTACCATCTCCAGCGCA	462	[14]
	CATAGTGGCTTCCCCGTCCACCTGCTCTA		
V_2 receptor	TACCTGCAGATGGTGGGCAT	581	[52]
	AGCAACACAAAGGGGGGTCT		
GAPDH	AGTCGGAGTGAACGGATTTGG	488	
	AGTTGTCATGGATGACCTTGG		

Solutions and drugs

A solution containing high K^+ (60 mM) was made by the isotonic replacement of Na^+ of HEPES-buffered NL with K^+. A Ca^{2+}-free solution was made by simply omitting $CaCl_2$ from the NL. A concentrated stock solution of cyclopiazonic acid (CPA), an inhibitor of the Ca^{2+}-ATPase of the intracellular Ca^{2+} store [79], at 10 mM were made in dimethyl sulfoxide and stored at -30˚C until use. A concentrated stock solution of [Arg^8]-Vasopressin (Peptide Institute, Osaka, Japan) at 0.1 mM, (d$(CH_2)_5^1$,Tyr(Me)^2,Arg^8)-Vasopressin, a receptor antagonist of V_1 and (d$(CH_2)_5^1$,Tyr(Me)^2,Thr^4,Orn^8,des-Gly-NH_2^9)-Vasotocin (dOVT), a receptor antagonist of OT (BACHEM, Bubendorf, Switzerland) at 1 mM were made in double distilled water and stored at -30˚C until use. All standard chemicals were from Sigma-Aldrich, St Louis, MO, USA, unless stated otherwise.

RESULTS

AVP-induced $[Ca^{2+}]_i$ signals and immunoreactivity against S-100 in DRG cell culture

At six days in culture, various cell types were present in our DRG culture, that was distinguishable on morphological criteria (Fig. 13D). The first type was roundly shaped and had highly dense cytosol, resembling the morphology of the DRG neurons [39] [39] (a), while a second type was represented by polygonal or spindle shaped cells with lower density cytosol in phase contrast microscopy (b). To identify on a functional basis the types of cells, we have used a 60 mM KCl (60 K^+) stimulation protocol (30 seconds) while performing $[Ca^{2+}]_i$ measurements. As illustrated in Fig. 13A and B, showing an example of the $[Ca^{2+}]_i$ changes in a typical filed of the DRG culture, only one cell responded with a $[Ca^{2+}]_i$ increase to the 60 K^+-induced depolarization. Panel C in Fig. 13 shows the response of the culture to the bath application of 1 μM AVP for 1 min after the exposure to 60 K^+ for 30 seconds. The majority of the cells responded with a clear Ca^{2+} signal, while the neuronal cells failed to respond. This difference in response is more clearly illustrated by the $[Ca^{2+}]_i$ traces in

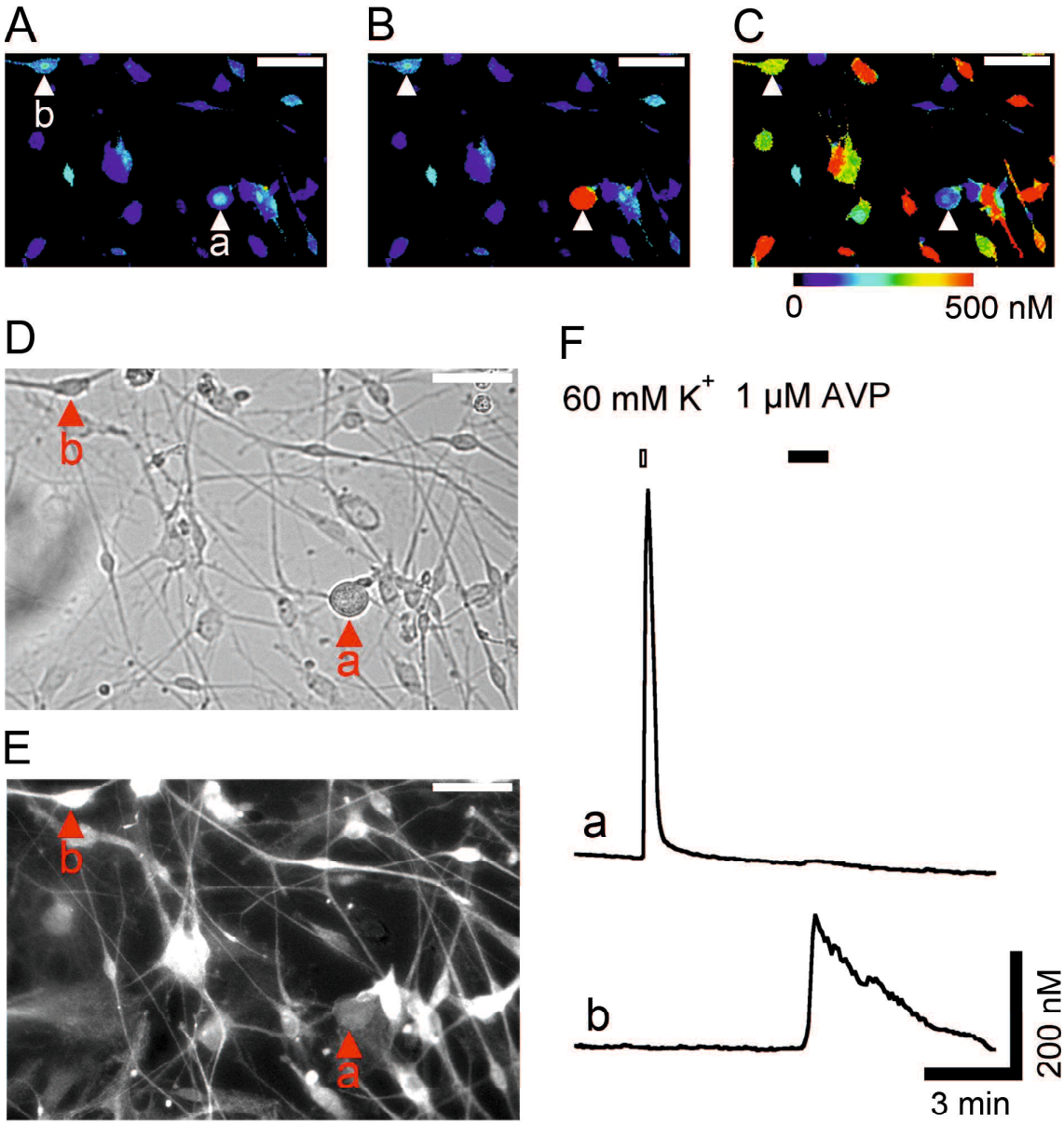
A
B
C
b
a
0
500 nM
D
b
a
E
b
a
F
60 mM K+ 1 μM AVP
a
b
200 nM
3 min
G
1
2
3
H
1
2
3

Fig. 13. $[Ca^{2+}]_i$ responses to high K^+ and AVP with S-100 antibody immuno-staining in rat cultured DRG cells. (A-C) Ca^{2+} imaging pseudo color pictures obtained in basal conditions (A), after 60 K^+ (B) and 1 μM AVP stimulations (C). (D) A bright field picture of the cells shown in A, B & C. (E) A fluorescence image obtained with anti S-100 antibody after the $[Ca^{2+}]_i$ dynamic measurement. (F) Time course of responses to K^+ and AVP obtained in the cells (a, b respectively). (G, H) Immunocytochemistry with an anti-S-100 antibody in DRG cells cultured for 7 days. Normal bright field images (G, H) of the same optical field are shown. Cells numbered 1-3 in G are shown with an expanded scale in H. Only the cell 2 showed S-100-immunopositive.Scale bars indicate 50 (A-G) and 100 μm (H). The results of (A-F) and (G, H) are obtained from the culture DRG cells at DIV 6 and DIV 3, respectively.

panels F, where in a neuron (a) only 60 K^+ evoked a rapid sharp rise in $[Ca^{2+}]_i$, whereas in a non-neuronal cell (b), only AVP evoked a long-lasting $[Ca^{2+}]_i$ increase.

In the DRG, there are two types of glial cells, the satellite glial cells and Schwann cells, and both show the expression of the S-100 protein [95]. Thus, to confirm the glial nature of the cells responding to AVP but not to 60 K^+ protocol in our DRG cultures on the basis of morphology and functional responses, we have performed immunocytochemical staining with an anti S-100 antibody on the coverslips previously used for $[Ca^{2+}]_i$ recording. As shown in the cell labeled 'b' in Fig. 13E, cells that responded to AVP were positively stained by the S-100 antibody. On the other hand, there was little S-100 immunoreactivity in the cell labeled 'a' that exhibited a transient rise in $[Ca^{2+}]_i$ to 60 K^+.

To investigate the relative abundance of the S-100-immunopositive non-neuronal cells, we performed specific immunocytochemistry on the cultures. Under our experimental conditions, 71% (392/575) of cells having morphology of non-neuronal cells positively stained with S-100 antibody (Fig. 13G,H). More importantly, of the S-100 positive cells, 74% (103/139) responded with a Ca^{2+} signal to the application of

AVP. Overall, these cells were quiescent in the absence of stimulation, without signs of any spontaneous activities, such as $[Ca^{2+}]_i$ oscillations, and showed, under our Ca^{2+} calibration conditions, a resting $[Ca^{2+}]_i$ of 33.9±1.8 nM (n = 832).

Dependence of AVP-evoked $[Ca^{2+}]_i$ rises on the culture period and the AVP concentrations

Maintenance of neural cells in primary cultures is usually associated with changes in the expression of various receptors, either as a function of the developmental stages or in response to the culture conditions [1, 16, 63]. To assess this possibility in our conditions, we have measured the amplitude of AVP-evoked (1 μM for 3 min) $[Ca^{2+}]_i$ responses and in cultures of different ages, between 0 and 10 DIV (days *in vitro*). For the sake of analysis, cells were divided into three groups depending on the amplitude of $[Ca^{2+}]_i$ increase in response to AVP: < 10 nM (i.e., non-respondent), 10-30 nM (small responses) and > 30 nM (large responses), and the relative proportion of these cell groups as a function of the age of the culture is plotted by columns in Fig. 14A. At DIV 0, 11% (35/331) of the cells showed

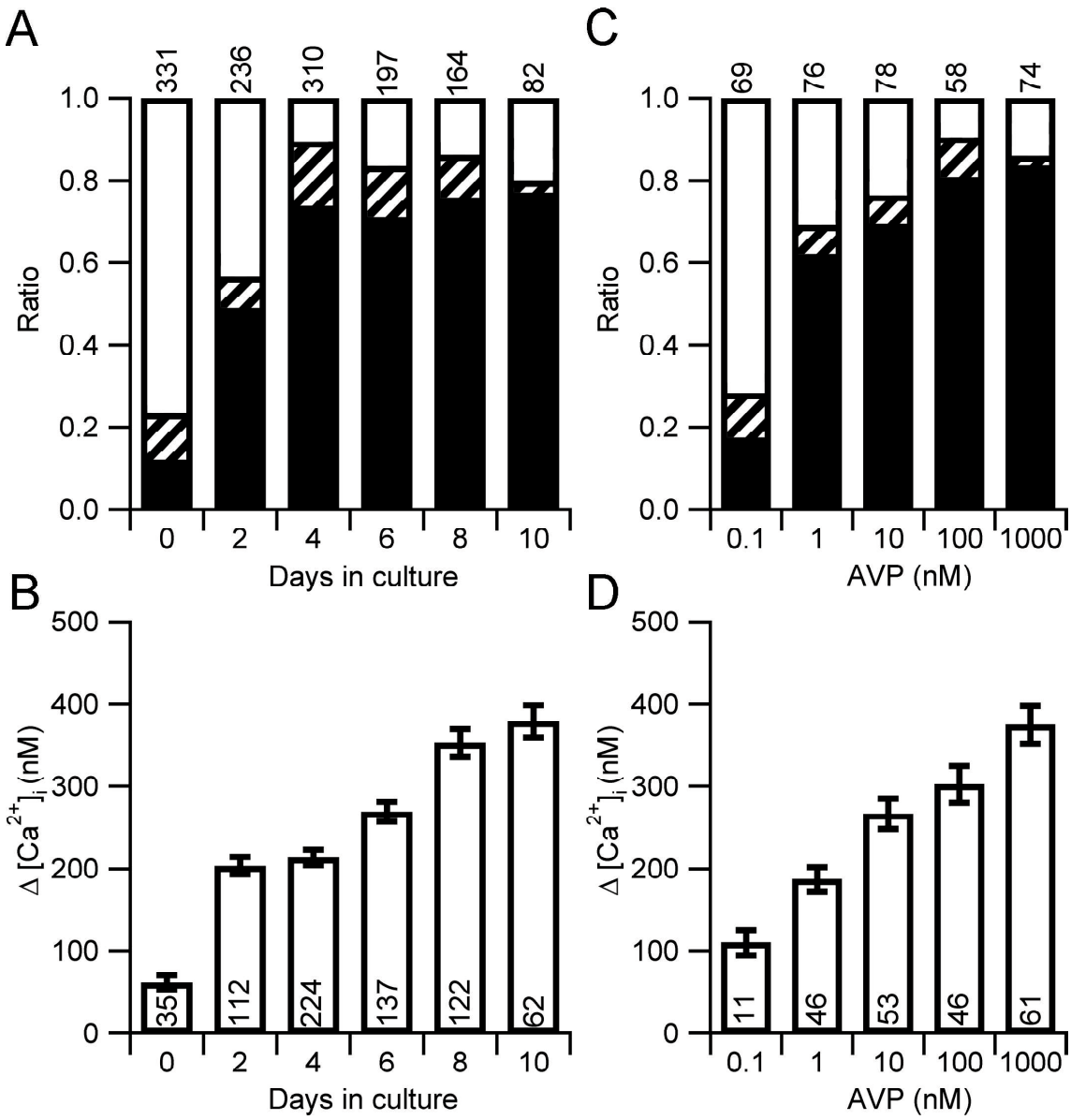
A
331
236
310
197
164
82
1.0
0.8
0.6
0.4
0.2
0.0
Ratio
0
2
4
6
8
10
Days in culture
C
69
76
78
58
74
0.1
1
10
100
1000
AVP (nM)
B
500
400
300
200
100
0
Δ [Ca2+]i (nM)
35
112
224
137
122
62
Days in culture
D
11
46
53
46
61
AVP (nM)

Fig. 14. Dependence of AVP-evoked $[Ca^{2+}]_i$ responses on the culture day and the concentration of AVP.

(A) Culture day dependence of AVP-evoked $[Ca^{2+}]_i$ responses in non-neuronal cells. Cells on each day of culture were divided into three groups depending on the amplitudes of the $[Ca^{2+}]_i$ responses as < 10 nM (open column), 10-30 nM (hatched column), and > 30 nM (solid column). (B) The mean amplitudes of the $[Ca^{2+}]_i$ responses in cells showing responses of > 30 nM in A are shown. The total numbers of the cells in this group are indicated in the columns. (C) Dose dependence of AVP-evoked $[Ca^{2+}]_i$ responses in non-neuronal cells at DIV 9. Cells were divided into three groups as in A and the relative proportion of the cells in each group is shown by columns. (D) The mean amplitudes of the $[Ca^{2+}]_i$ responses in the cells showing responses of > 30 nM in C are shown. The total numbers of the cells in this group are indicated in the columns. The amplitude of the $[Ca^{2+}]_i$ responses ($\Delta[Ca^{2+}]_i$) was calculated by subtracting the basal level from the peak amplitude of the evoked responses.

responses larger than 30 nM, but the proportion of cells in this group gradually increased with the age in culture until DIV 4, and reached 72% (224/310). From the DIV 4 to DIV 10, the ratio of this group remained stable (approximately 70%). The average amplitudes of $[Ca^{2+}]_i$ responses in cells in the group showing responses larger than 30 nM in Fig. 14A are illustrated in Fig. 14B, demonstrating that the amplitude of the AVP-induced $[Ca^{2+}]_i$ response in the non-neuronal cells increased with culture age.

To examine the relationship between the concentration of AVP and the amplitude of the $[Ca^{2+}]_i$ responses, effects of AVP at different concentrations varying between 0.1 and 1000 nM on $[Ca^{2+}]_i$ were examined. To minimize the influence of the culture age on the amplitudes of AVP-induced responses, only DIV 9 cells were used in this experiment. Responses in individual cells were divided into three groups as Fig. 14A. Even at the low concentration (0.1 nM) of AVP, 16% of the cells showed $[Ca^{2+}]_i$ responses larger than 30 nM (Fig. 14C). The proportion of cells showing responses with the amplitude of larger than 30 nM gradually increased in a concentration-dependent manner. Figure 14D shows the averaged amplitudes of the AVP-induced $[Ca^{2+}]_i$ increase in the group of the cells showing responses exceeding 30 nM as in Figure 14C. The amplitudes also

increased in a concentration-dependent manner.

$[Ca^{2+}]_i$ responses to repetitive stimulations with AVP

Assessment of the main parameters of Ca^{2+} homeostasis requires, in some experimental paradigms, repeated exposures to the activator agent. It has been shown previously that in the SON-AVP neurons, the $[Ca^{2+}]_i$ response to repeated stimulations with AVP shows desensitization [17]. A similar protocol was adopted in this study, involving 3 repetitive applications of a low, concentration of AVP (at 1 nM for 3 min), separated by 20 min intervals (Fig. 15A). Twenty-six out of 30 cells showed a good $[Ca^{2+}]_i$ response (i.e., larger than 30 nM) to all 3 repetitive applications of AVP. However, the $[Ca^{2+}]_i$ responses after the 1^{st} and 2^{nd} AVP applications were smaller suggesting a desensitization of the AVP receptors. The amplitudes of the $[Ca^{2+}]_i$ responses to the 1^{st}, 2^{nd} and 3^{rd} stimulations were 231 ± 24 nM, 138 ± 9 nM, 90 ± 15 nM, respectively (n = 30) and significantly different (1^{st} and 2^{nd}, $P < 0.01$ by ANOVA; 2^{nd} and 3^{rd}, $P < 0.05$ by ANOVA). Relative amplitudes of the responses to those evoked by the first stimulation are shown in Fig. 15B.

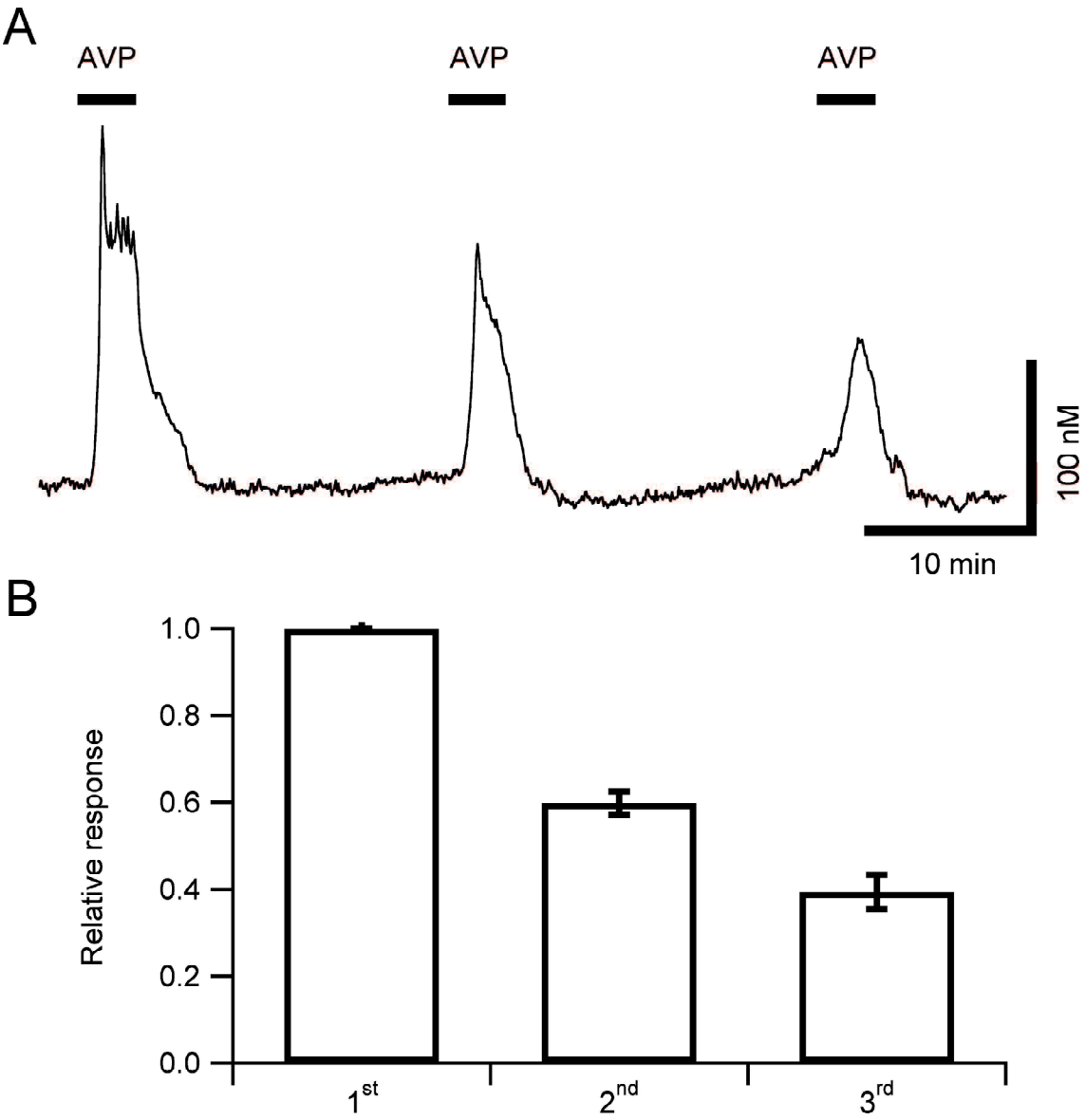

Fig. 15. Effect of repetitive AVP stimulation on $[Ca^{2+}]_i$ in non-neuronal cells obtained from the DRG culture.

(A) Representative traces of $[Ca^{2+}]_i$ responses to 3 repetitive AVP applications (3 min each) with 20 min interval. (B) Summarized results showing an amplitude decay of the $[Ca^{2+}]_i$ responses obtained from 30 non-neuronal cells. The amplitude of the $[Ca^{2+}]_i$ responses (from the basal level to the peak) was normalized to the 1st $[Ca^{2+}]_i$ response and the values are shown as the mean ± SEM.

The source of Ca^{2+} in response to AVP

To clarify the origin of Ca^{2+} in response to AVP in the non-neuronal cells from DRG cultures, experiments were first performed to assess the response to AVP in the absence of external Ca^{2+}. For these experiments, cells were first stimulated with 1 nM AVP for 3 min (as shown in Fig. 16A) in the NL containing 2 mM $CaCl_2$ and then perfused with Ca^{2+}-free solution prior to 2nd application of AVP. The NL was then reintroduced as shown in the traces (Fig. 16). While data in Fig. 15B, show that the second AVP exposure induces a $[Ca^{2+}]_i$ response that is 60 ± 2.7 %, in the absence of external Ca^{2+}, the second response was 52 ± 3 % (n=40), a value that was not significantly different ($P > 0.05$ by Student's *t*-test) from that recorded in the presence of Ca^{2+} (Fig. 16C), indicating that the AVP-induced Ca^{2+} signal originates in the intracellular Ca^{2+} compartments.

This is further supported in experiments using CPA, a drug known to block the reuptake of Ca^{2+} into the endoplasmic reticulum Ca^{2+} stores, but also to release Ca^{2+} from these stores in a manner controlled by the resting levels of $InsP_3$ [4]. In these experiments, CPA (10 μM) alone, in the absence of external Ca^{2+},

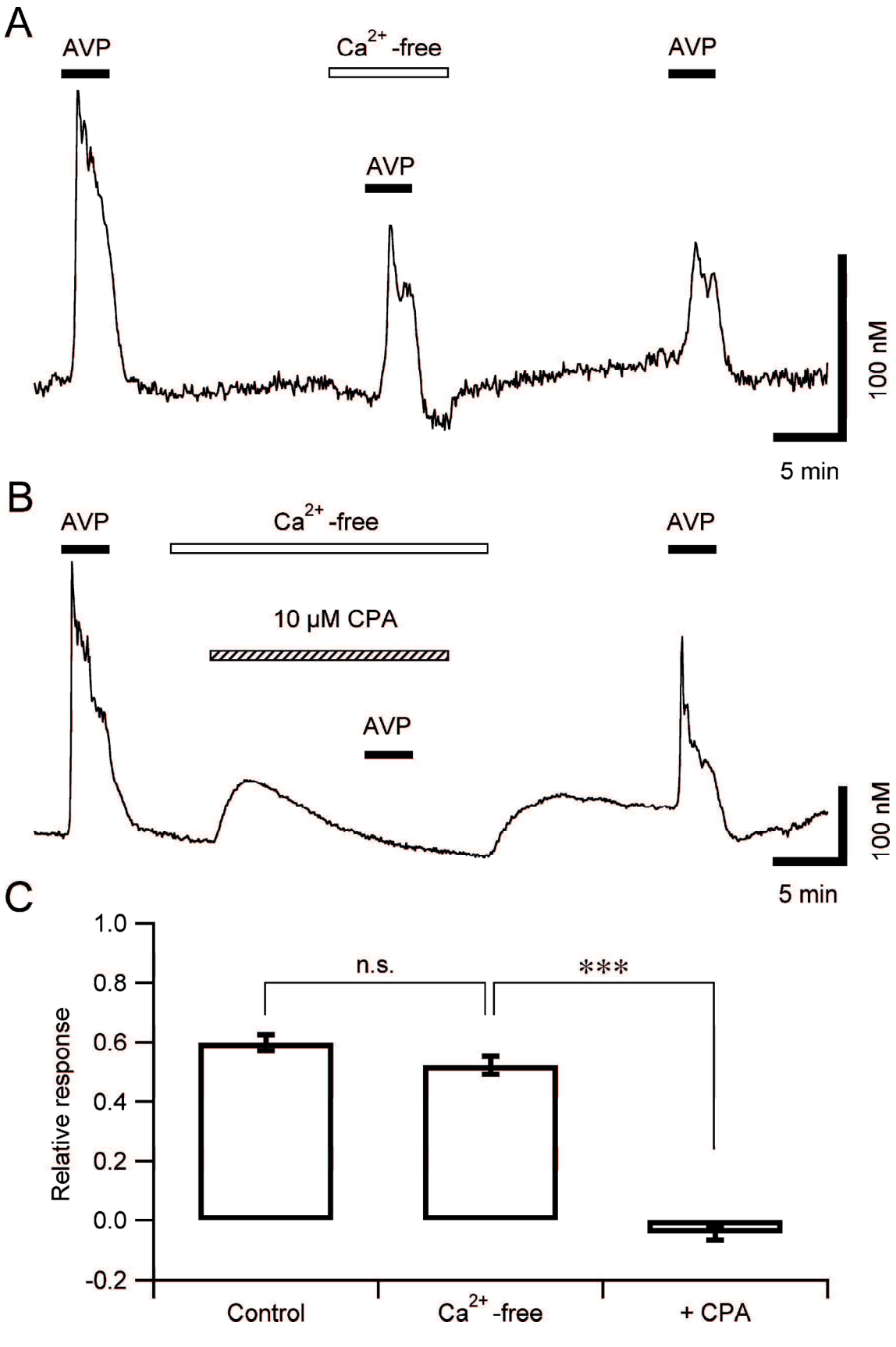
A
AVP
Ca2+ -free
AVP
AVP
100 nM
5 min
B
AVP
Ca2+ -free
AVP
10 μM CPA
AVP
100 nM
5 min
C
Relative response
1.0
0.8
0.6
0.4
0.2
0.0
-0.2
n.s.
***
Control
Ca2+ -free
+ CPA

Fig. 16. Involvement of external and intracellular Ca^{2+} in the AVP response.
This panel displays the effects of low external Ca^{2+} and the sarco-endpalsmic reticulum Ca^{2+} ATPase inhibitor, CPA, on $[Ca^{2+}]_i$ responses to AVP in non-neuronal cells.
(A) A representative trace showing $[Ca^{2+}]_i$ responses to AVP (1 nM) before, during, and after perfusion with Ca^{2+} free solution. (B) A representative example of $[Ca^{2+}]_i$ responses to AVP (1 nM) before, during, and after perfusion with CPA-containing Ca^{2+}-free solution. (C) Summarized results showing $[Ca^{2+}]_i$ responses to AVP obtained in control (n = 30), Ca^{2+} free (n = 40), and Ca^{2+} free with CPA (n = 25). Summarized data of control are obtained from the result of second time application of AVP in Fig. 3. The values are shown as the mean ± SEM. The $[Ca^{2+}]_i$ responses are expressed as relative responses in comparison to the 1st AVP-induced peak in each experiment (***: $P<0.001$).

induced an sustained increase in $[Ca^{2+}]_i$, indicating of a release from the intracellular Ca^{2+} stores (Fig. 16B); and in these conditions AVP failed to initiate any $[Ca^{2+}]_i$ increase. However, when the Ca^{2+} concentration in the bath solution was restored to 2 mM, there was a prolonged rise in $[Ca^{2+}]_i$, which indicates a sustained store-operated Ca^{2+} entry (SOCE) was evoked, and the Ca^{2+} stores were refilled. In such conditions, a further AVP application is able to generate a transient $[Ca^{2+}]_i$ response; and these results are summarized in Fig. 16C.

The final indication that AVP generates a Ca^{2+} signal mediated by intracellular signaling involving $InsP_3$ and subsequent intracellular Ca^{2+} release, comes from experiments using modulators of phospholipase C (PLC) activity. The compound U73122 has been used extensively as a relatively specific inhibitor of PLC [74], while the related compound U73343 has no inhibitory activity [83]. The cultures were thus exposed to AVP, and then pre-incubated with U73122 for 3 min prior to the 2nd AVP administration (Fig. 17A). While U73122 addition did not affected the levels of resting Ca^{2+}, it significantly reduced the AVP-evoked $[Ca^{2+}]_i$ rises (Fig. 17A and C); Fig. 17B and C shows that the non-specific agent U73343 had no effect.

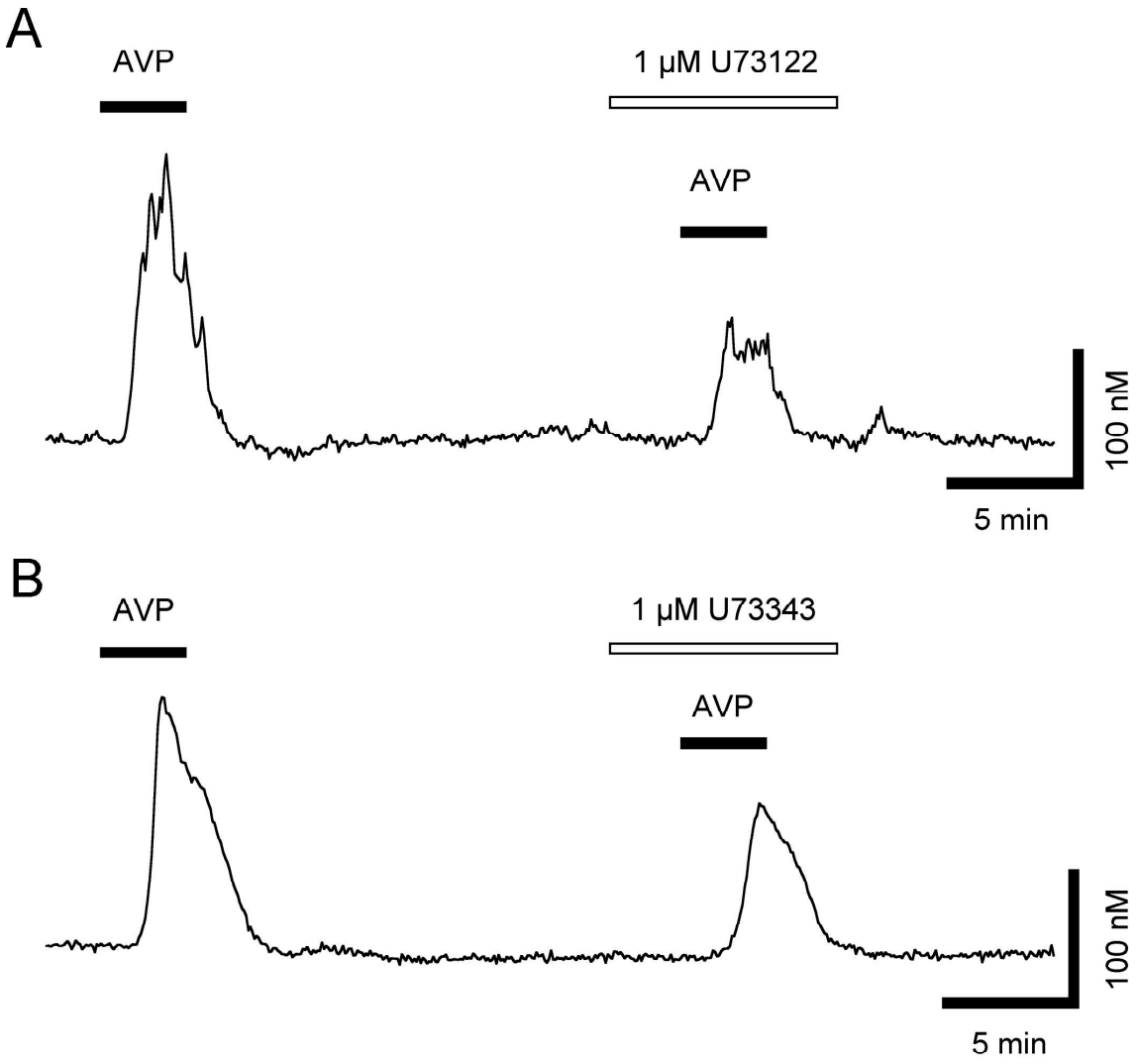
A
AVP
1 μM U73122
AVP
100 nM
5 min
B
AVP
1 μM U73343
AVP
100 nM
5 min

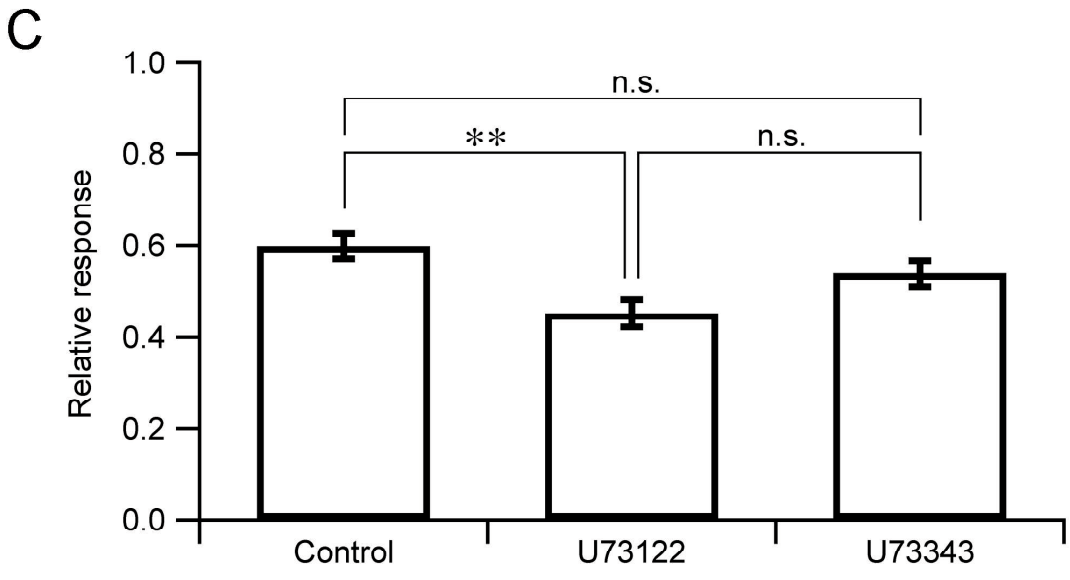
C
Relative response
1.0
0.8
0.6
0.4
0.2
0.0
n.s.
**
n.s.
Control
U73122
U73343

Fig. 17. The possibility of PLC participation in the $[Ca^{2+}]_i$ responses evoked by AVP. This panel displays the effects of the PLC inhibitor, U73122 and inactive analog of U73122, U73343 on $[Ca^{2+}]_i$ responses to AVP in non-neuronal cells.
(A), (B) Representative traces of $[Ca^{2+}]_i$ responses to AVP (1 nM) in the presence of U73122 (1 μM) or U73343 (1 μM). (C) Summarized results showing $[Ca^{2+}]_i$ responses to AVP obtained in U73122 (n = 48), and U73343 (n = 30). The values are shown as the mean ± SEM. The $[Ca^{2+}]_i$ responses are expressed as relative responses in comparison to the 1st AVP-induced peak in each experiment (**: P<0.01).

The subtype of AVP receptors contributing to the $[Ca^{2+}]_i$ rises

In order to examine whether AVP-induced $[Ca^{2+}]_i$ responses in non-neuronal cells of DRG cell cultures are mediated by specific AVP receptors, we then pharmacologically targeted the subtypes of AVP receptor contributing to the $[Ca^{2+}]_i$ response by use of the V_1 receptor antagonist, $(d(CH_2)_5^1,Tyr(Me)^2,Arg^8)$-Vasopressin. Initially the cells were stimulated with a low AVP concentration (at 1 nM for 3 min) to identify the AVP-responsive cells; subsequently cells were stimulated by a much larger AVP concentration (1 μM, 3 min, n=25, control) (Fig. 18A). The rationale for the use of a much larger concentration of AVP for the secondary exposure was to counteract the desensitization effect. To test the effect of the antagonist, the cells were perfused with $(d(CH_2)_5^1,Tyr(Me)^2,Arg^8)$-Vasopressin at 100 nM for 3 min before the 2^{nd} AVP stimulation, and continuously perfused further for 9 min. $(d(CH_2)_5^1,Tyr(Me)^2,Arg^8)$-Vasopressin alone had no effect on resting $[Ca^{2+}]_i$.

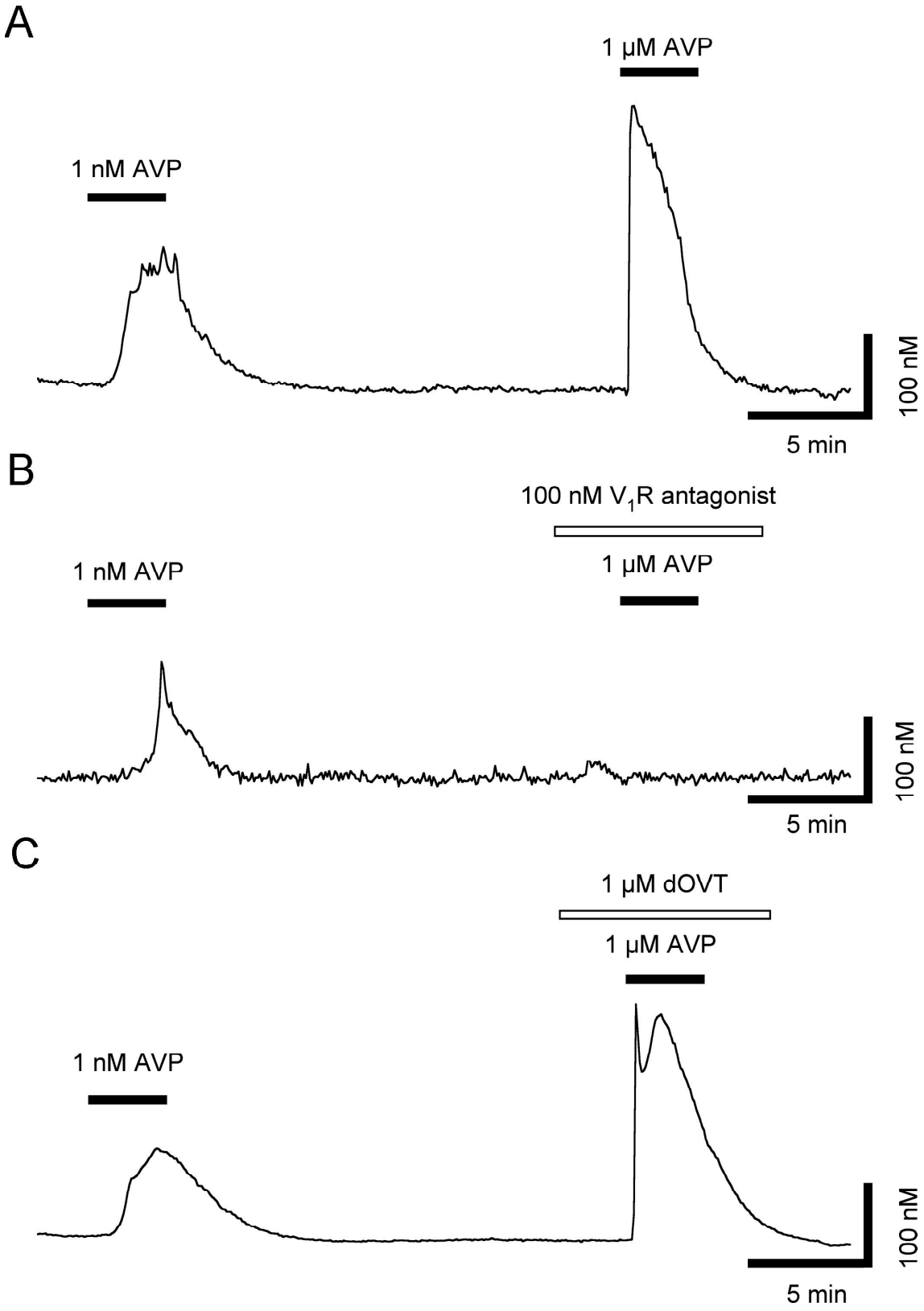
A
1 µM AVP
1 nM AVP
100 nM
5 min
B
100 nM V1R antagonist
1 µM AVP
1 nM AVP
100 nM
5 min
C
1 µM dOVT
1 µM AVP
1 nM AVP
100 nM
5 min

Figure 18. A specific subtype of vasopressin receptor mediates AVP-induced Ca^{2+} transients.

This panel displays the effects of the V_1 receptor antagonist, $(d(CH_2)_5{}^1,Tyr(Me)^2,Arg^8)$-Vasopressin, and the effects of the OT receptor antagonist, dOVT, on $[Ca^{2+}]_i$ responses to AVP in non-neuronal cells.

(A) Typical traces of $[Ca^{2+}]_i$ responses to AVP (1 nM and 1 μM) administered with 20 min intervals. (B) Representative traces of $[Ca^{2+}]_i$ responses to AVP (1 μM) in the presence of V_1 receptor antagonist, $(d(CH_2)_5{}^1,Tyr(Me)^2,Arg^8)$-Vasopressin (100 nM) (n = 25) or an OT receptor antagonist, dOVT (1 μM) (C) (n = 34).

In the presence of the antagonist, the $[Ca^{2+}]_i$ response evoked by AVP was completely abolished in all cells recorded (n = 18, Fig. 18B) and there was a significant difference between the amplitudes of AVP-evoked $[Ca^{2+}]_i$ responses in control cells and the ones obtained in the cells treated with $(d(CH_2)_5^1,Tyr(Me)^2,Arg^8)$-Vasopressin (tested by Student's t test; $P<0.05$).

Since AVP at higher concentrations was shown to activate oxytocin (OT) receptors [12], we also examined the specificity of the involvement of AVP receptors by using the OT receptor antagonist, dOVT, on the $[Ca^{2+}]_i$ responses evoked by AVP in non-neuronal cells. Using the same protocols as, application of dOVT did not affect the AVP-evoked Ca^{2+} signal (tested by Student's t test; $P>0.05$ vs. control) (n = 34, Fig. 18C) suggesting the specificity of action of AVP in non-neuronal cells in DRG.

To clarify the subtype of vasopressin receptors expressed in the DRG, RT-PCR was carried out. As shown in Fig. 19A, PCR products corresponding to V_{1a} and V_{1b} cDNAs were observed when using samples from rat DRG tissues, but no signal was detected with the V_2 receptor primers. Because amplitudes of $[Ca^{2+}]_i$ responses evoked by AVP increased during culture days in our study (Fig. 19B), we also examined

culture-day-dependent changes in expressions of mRNAs in cultured DRG cells (Fig. 19B). V_{1a} receptor mRNA was expressed in cultured DRG cells at DIV 0, 5 and 10. In contrast, weak signal of V_{1b} mRNA in cells at DIV 0 and 5 was observed weakly and no signal was detected in cells at DIV 10.

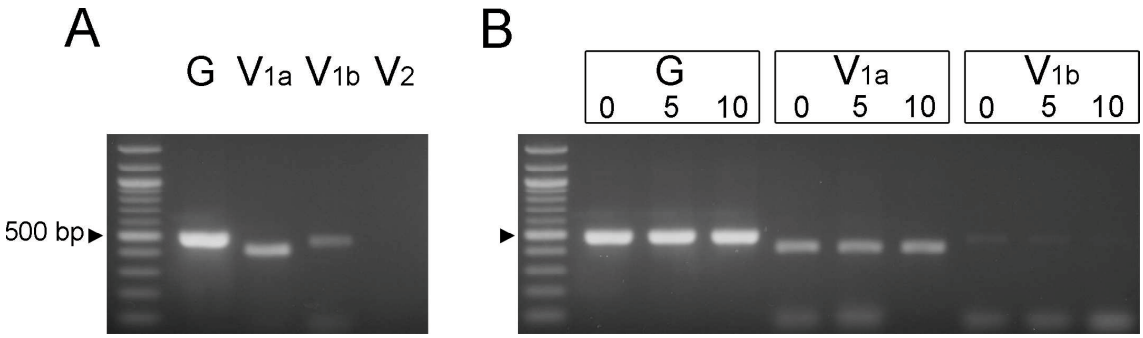

Fig. 19. The expression of AVP receptor mRNAs in DRG tissues and cultured DRG cells.

(A) The expression of V_{1a}, V_{1b} and V_2 receptor mRNAs in rat DRG tissue was analyzed by RT-PCR using the specific primers listed in Table 4. (B) The expression of GAPDH (G), V_{1a} and V_{1b} receptor mRNAs in cultured DRG cells at DIV 0, 5 and 10.

DISCUSSION

Although the presence of AVP and of a neuropeptidergic system in DRG has been known for some time [31, 36] there are no detailed studies of the possible effects and signaling pathways evoked by involvement AVP. Therefore the purpose of this work was to elucidate how various types of DRG cells, specifically non-neuronal cells, could respond to the challenges of AVP in terms of Ca^{2+} handling.

AVP induces $[Ca^{2+}]_i$ transients in cultured DRG glial cells

We demonstrated that DRG cells showed rapid $[Ca^{2+}]_i$ responses to AVP in a concentration-dependent manner in the physiological range. The results of the immunocytochemical staining in combination with the $[Ca^{2+}]_i$ measurement revealed that the majority of the non-neuronal cells having high sensitivity to AVP in the DRG was S-100-immunopositive. It has been reported that the two types of glial cells in the DRG are S-100-immunopositive [95]. Taken together, it is considered the cells that did not respond to 60 K^+ but responded to AVP in the present study are most likely to be either satellite glial cells or Schwann cells.

The minimum effective concentrations of AVP causing $[Ca^{2+}]_i$ responses were 100 pM in non-neuronal cells in DRG culture. This concentration is close to that reported for AVP-evoked $[Ca^{2+}]_i$ responses in hippocampal and cortical astrocytes [87].

AVP receptor subtype

Our pharmacological approach led us to identify important features of the $[Ca^{2+}]_i$ response evoked by AVP. This response shows a significant desensitization. The AVP-evoked $[Ca^{2+}]_i$ response was completely blocked by the selective V_1 antagonist, $(d(CH_2)_5{}^1,Tyr(Me)^2,Arg^8)$-Vasopressin, and unaffected by the selective OT receptor antagonist, dOVT, indicating that AVP receptors mediating the $[Ca^{2+}]_i$ response are the V_1 subclass. The AVP-evoked $[Ca^{2+}]_i$ response showed clear desensitization when AVP was administered repeatedly. The results are consistent with previous reports that cellular responses via V_1 AVP receptors undergo strong desensitization in AVP-evoked $[Ca^{2+}]_i$ responses from smooth muscle cells of rat aorta [9, 76] porcine retinal arteries [10], secretory responses from ovine pituitary corticotrophs [28, 29], and SON-AVP neurons [17, 25].

V_{1a} and V_{1b} PCR products were observed when using samples from DRG tissues, suggesting that both V_{1a} and V_{1b} receptor mRNAs are expressed in rat DRG tissues. In cultured DRG cells prepared by the same method as used for cell isolation for the $[Ca^{2+}]_i$ measurement, clear V_{1a} PCR products were observed sustainably during the culture days, but a weak V_{1b} PCR signal was observed at DIV 0 and 5, and no signal was observed at DIV10. Considering the larger $[Ca^{2+}]_i$ responses in the later culture days, these results indicate that the AVP receptor subtype responsible for the $[Ca^{2+}]_i$ responses in rat DRG culture cells may be the V_{1a} subtype.

Signal transduction mechanism of AVP receptors in the DRG

The V_1 receptor is known to be coupled to Gq/11 proteins, which activate PLC and lead to the production of $InsP_3$ [97]. Several lines of the argument supports the view that the AVP-evoked Ca^{2+} signals in the DRG glial cells are mediated by an $InsP_3$-dependent signaling pathway: i) the response was not affected by the removal of extracellular Ca^{2+} but ii) abolished by the release from the intracellular Ca^{2+} stores with CPA, and iii) the PLC blocker U-73122 inhibited AVP-evoked $[Ca^{2+}]_i$ rises. Presence of PLC has been

reported in DRG neurons [26, 34, 43] with all the major PLC isoforms beta1, beta3 and beta4 being expressed, although there appear to be a prevalence of the beta3 isoform [26], which has been shown to play a critical role in neuropathic pain in mouse and human DRG [81]. The present results indicate the existence PLC also in the DRG glial cells, although little is known about the isoform expressed.

The Gq-PLC-$InsP_3$ mechanism is well known to evoke $InsP_3$-dependent Ca^{2+} release from intracellular Ca^{2+} stores, and Ca^{2+} store depletion due to massive Ca^{2+} release has been shown to activate store-operated Ca^{2+} entry (SOCE) through plasma membrane Ca^{2+} channels [67]. The present results that a prolonged $[Ca^{2+}]_i$ increase was observed upon CPA removal and extracellular Ca^{2+} restoration indicates such mechanism is present also in DRG glial cells. Activation of SOCE could be one of the reasons why AVP-evoked $[Ca^{2+}]_i$ responses in glial cells showed very slow recovery when a high concentration of AVP was applied (Fig. 1F).

Possible physiological roles of AVP in DRG

The probable sources of AVP to activate V_1 receptors of non-neuronal cells in the

DRG are the neurons themselves [36] but the circulating AVP could also have an effect. It has been documented that, in the hypophysial portal blood, the plasmatic AVP concentration is around 0.5 nM [51]. In other models, Lee and collaborators reported a physiological concentration of AVP of 50-100 pg/ml (46-92 pM) in the heart [47], and physiological effects of AVP were seen at 3-30 pM in the pancreas of the rat [102]. Circulating AVP concentration changes mainly during dehydration and it has been reported that over 48-72 h of dehydration condition, plasma AVP concentration increases more than 10 times above basal levels [84, 88]. Therefore it would be plausible that AVP concentrations similar to those used in our study to elicit Ca^{2+} signals could be found in physiological states. If AVP was released from DRG neurons themselves, the AVP concentration in the DRG would reach a much higher level than that discussed above, and thus be even more likely to induce a Ca^{2+} signal in neighboring glial cells.

Local functional regulation by small peptidetgic signaling is not uncommon. Bradykinin (BK), another nonapeptide, has been shown to cause a $[Ca^{2+}]_i$ signal in DRG Schwann cells, with a release of glutamate and aspartate [68]. The BK-evoked increase of $[Ca^{2+}]_i$ in satellite glial cells from postnatal DRG also activate a Ca^{2+}-dependent Cl^-

conductance, with a putative participation in the inflammatory process [23]. Moreover, AVP has been shown to elevate $[Ca^{2+}]_i$ and release glutamate in hippocampal and cortical astrocytes of rats [87]. Whether or not AVP can have similar effects and induce a glial release of bioactive substances in the DRG remains to be determined.

In the present study, the amplitude of $[Ca^{2+}]_i$ responses evoked by AVP (1 μM) increased with an increase in the culture time. Even under an acute condition (day 0), about 10 % of cells examined showed $[Ca^{2+}]_i$ responses larger than 30 nM upon AVP application, indicating that the AVP-mediated $[Ca^{2+}]_i$ response of glial cells in the DRG could exist also *in vivo*. Moreover, if AVP was released from neighboring DRG neurons, the concentration of AVP would reach a level much higher than the level of AVP in the systemic circulation discussed above, and it would be sufficient to evoke the $[Ca^{2+}]_i$ response in DRG glial cells. At day 0, the mean amplitude of $[Ca^{2+}]_i$ responses obtained from the group showing responses larger than 30 nM was six times smaller than that obtained at day 10. The differences in the amplitudes of the $[Ca^{2+}]_i$ responses due to culturing time could result from differences in the expression density of the AVP V_1 receptor on the plasma membrane. There are at least two possibilities that the density of

V_1 receptor expressed at day 0 could be low: 1) V_1 receptors are highly expressed on the glial cells *in vivo* but internalized or damaged during the enzymatic and mechanical digestions, and recover during cell culture; 2) The density of V_1 receptors expressed on the glial cells increases during the day of cell culture. Our RT-PCR results showed that V_{1a} receptor mRNA was strongly expressed both in DRG tissues and in cultured DRG cells even at culture day 0, and that there was no evident change in the expression during culture. These results support the first possibility.

With this communication we show that the neuropeptide AVP generates Ca^{2+} signals in DRG glial cells, in a concentration-dependent and receptor-specific manner. This suggests that the vasopressinergic molecular machinery could play a role in the physiology and/or pathophysiology of the peripheral sensory system.

CONCLUDING REMARKS

It was demonstrated in the Chapter 1 that only AVP (but not OT) neurons in the rat SON express the osmoreceptor, and that the osomoreceptor is composed of, at least in part, full-length TRPV1. The osmoreceptor in the rat SON may be a heterotetramer in which full-length TRPV1 is co-assembled with some other, yet identified, molecules, because several clear differences exist in the functional properties between the rat TRPV1 and the osmoreceptor in the rat SON. The molecule that is co-assembled with full-length TRPV1 could be TRPV1_SON, a new splice valiant of TRPV1 that is newly identified in this study. Further studies are needed to elucidate the molecular and cellular identity of the osmoreceptor in SON neurons and other neurons in the central nervous system.

It was also revealed in the Chapter 2 that AVP induces a $[Ca^{2+}]_i$ increase by causing an $InsP_3$-evoked release of Ca^{2+} from intracellular Ca^{2+} stores in rat DRG glial cells via AVP V_{1a} receptor. Physiological and/or pathophysiological roles of AVP in the DRG will be elucidated in future studies.

More than 60 years have already passed since the amino acid sequence of AVP was reported. Thousands of studies on AVP have been reported since the

discovery of this physiologically important neuropeptide, and this thesis has added two new pieces of evidence with regard to the mechanism of AVP secretion and the effect of AVP on DRG glial cells. It is expected that these new pieces of evidence will accelerate the research on physiology and pathophysiology of AVP further.

ACKNOWLEDGEMENTS

I would like to express my sincere gratitude to my supervisor, Dr. Izumi Shibuya, Professor, Joint Department of Veterinary Medicine, Faculty of Agriculture, Tottori University, Japan, for providing me this precious study opportunity as a Ph.D student in his laboratory.

I especially would also like to express my deepest appreciation to my supervisor, Dr. Naoki Kitamura, Associate professor, Joint Department of Veterinary Medicine, Faculty of Agriculture, Tottori University, Japan, for his elaborated guidance, considerable encouragement and invaluable discussion that make my research of great achievement and my study life unforgettable.

I sincerely wish to appreciate Dr. Alexei Verkhratsky, University of Manchester, School of Biological Sciences, Oxford Road, Manchester, UK, Professor, Dr. Govindan Dayanithi, Professor, Department of Molecular Neurophysiology, Institute of Experimental Medicine, Academy of Science of the Czech Republic, Prague, Czech Republic, Dr. Cedric Viero, Senior Research Associate, Department of Experimental and Clinical Pharmacology and Toxicology, Medical Faculty, Saarland University,

Homburg, Germany, Dr. Emil Toescu, Associate Professor, Department of Physiology, School of Medicine, Birmingham University, UK, Dr. Yasuaki Kawasaki, Professor, Department of Behavioral Physiology and ecology, Joint Faculty of Veterinary Medicine, Kagoshima University, Japan, Dr. Kenji Takahashi, Associate professor, Joint Department of Veterinary Pharmacology, Faculty of Agriculture, Tottori University, Japan, Dr. Atsushi Asano, Associate professor, Joint Department of Veterinary Biochemistry, Faculty of Agriculture, Tottori University, Japan, and Dr. Yoshinao Hosaka, Professor, Joint Department of Veterinary Anatomy, Faculty of Agriculture, Tottori University, Japan for their intimate advice and comments to my research projects and thesis.

I am very grateful also to Dr. Tomohiko Kayano, Postdoctoral fellow, Department of Molecular Neurophysiology, Institute of Experimental Medicine, Academy of Science of the Czech Republic, Prague, Czech Republic, Oksana Forostyak, PhD course student, Department of Molecular Neurophysiology, Institute of Experimental Medicine, Academy of Science of the Czech Republic, Prague, Czech Republic, Rina Shibasaki, Heart Animal Clinic, Aichi, Japan, Nami Takebuchi, Lion Corporation, Tokyo, Japan,

Momoko Ichimura, Kyoto prefecture, Kyoto, Japan and the students in this laboratory for their valuable cooperation in my experiments.

This study was supported by a research grant from KAKENHI (Grant #: 18380175, 25450464), and Grant-in-Aid for JSPS Fellows. Dr. G.Dayanithi is supported by Japan Society for the Promotion of Science Invitation Fellowship Program (ID#FY2008; S-08216).

I would like to extend my indebtedness to my family for their endless love, understanding, support, encouragement and sacrifice throughout my study.

Finally, I would like to thank and pay my respects to animals for giving excellent data in my study.

REFERENCE

[1] A.Y. Abramov, M.R. Duchen, Impaired mitochondrial bioenergetics determines glutamate-induced delayed calcium deregulation in neurons, Biochim Biophys Acta, 1800 (2010) 297-304.

[2] L.K. Bak, A. Schousboe, H.S. Waagepetersen, The glutamate/GABA-glutamine cycle: aspects of transport, neurotransmitter homeostasis and ammonia transfer, J Neurochem, 98 (2006) 641-653.

[3] P.H. Baylis, Osmoregulation and control of vasopressin secretion in healthy humans, Am J Physiol, 253 (1987) R671-678.

[4] M. Bentley, D.C. Nycz, A. Joglekar, I. Fertschai, R. Malli, W.F. Graier, J.C. Hay, Vesicular calcium regulates coat retention, fusogenicity, and size of pre-Golgi intermediates, Mol Biol Cell, 21 (2010) 1033-1046.

[5] I.F. Bielsky, S.B. Hu, K.L. Szegda, H. Westphal, L.J. Young, Profound impairment in social recognition and reduction in anxiety-like behavior in vasopressin V1a receptor knockout mice, Neuropsychopharmacology, 29 (2004) 483-493.

[6] E.A. Bone, P. Fretten, S. Palmer, C.J. Kirk, R.H. Michell, Rapid accumulation of inositol phosphates in isolated rat superior cervical sympathetic ganglia exposed to V1-vasopressin and muscarinic cholinergic stimuli, Biochem J, 221 (1984) 803-811.

[7] C.W. Bourque, Central mechanisms of osmosensation and systemic osmoregulation, Nat Rev Neurosci, 9 (2008) 519-531.

[8] M.J. Brimble, R.E. Dyball, M.L. Forsling, Oxytocin release following osmotic activation of oxytocin neurones in the paraventricular and supraoptic nuclei, J Physiol, 278 (1978) 69-78.

[9] V.A. Briner, B. Williams, P. Tsai, R.W. Schrier, Demonstration of processing and recycling of biologically active V1 vasopressin receptors in vascular smooth muscle, Proc Natl Acad Sci U S A, 89 (1992) 2854-2858.

[10] C. Caramelo, P. Tsai, K. Okada, V.A. Briner, R.W. Schrier, Mechanisms of rapid desensitization to arginine vasopressin in vascular smooth muscle cells, Am J Physiol, 260 (1991) F46-52.

[11] M.J. Caterina, M.A. Schumacher, M. Tominaga, T.A. Rosen, J.D. Levine,

D. Julius, The capsaicin receptor: a heat-activated ion channel in the pain pathway, Nature, 389 (1997) 816-824.

[12] B. Chini, M. Manning, Agonist selectivity in the oxytocin/vasopressin receptor family: new insights and challenges, Biochem Soc Trans, 35 (2007) 737-741.

[13] S. Choi-Kwon, A.J. Baertschi, Splanchnic osmosensation and vasopressin: mechanisms and neural pathways, Am J Physiol, 261 (1991) E18-25.

[14] M. Chritin, P. Roquette, M.F. Schulz, C. Breton, E. Tribollet, Up-regulation of vasopressin V(1a) receptor mRNA in rat facial motoneurons following axotomy, Brain Res Mol Brain Res, 70 (1999) 210-218.

[15] S. Ciura, W. Liedtke, C.W. Bourque, Hypertonicity sensing in organum vasculosum lamina terminalis neurons: a mechanical process involving TRPV1 but not TRPV4, J Neurosci, 31 (2011) 14669-14676.

[16] C. Costantini, E. Lorenzetto, B. Cellini, M. Buffelli, F. Rossi, V. Della-Bianca, Astrocytes regulate the expression of insulin-like growth

factor 1 receptor (IGF1-R) in primary cortical neurons during in vitro senescence, J Mol Neurosci, 40 (2010) 342-352.

[17] G. Dayanithi, H. Widmer, P. Richard, Vasopressin-induced intracellular Ca2+ increase in isolated rat supraoptic cells, J Physiol, 490 (Pt 3) (1996) 713-727.

[18] G. Dayanithi, C. Viero, I. Shibuya, The role of calcium in the action and release of vasopressin and oxytocin from CNS neurones/terminals to the heart, J Physiol Pharmacol, 59 Suppl 8 (2008) 7-26.

[19] G. Dayanithi, O. Forostyak, Y. Ueta, A. Verkhratsky, E.C. Toescu, Segregation of calcium signalling mechanisms in magnocellular neurones and terminals, Cell Calcium, 51 (2012) 293-299.

[20] C. Deleuze, A. Duvoid, N. Hussy, Properties and glial origin of osmotic-dependent release of taurine from the rat supraoptic nucleus, J Physiol, 507 (Pt 2) (1998) 463-471.

[21] J. Dine, V.R. Ducourneau, V.S. Fenelon, P. Fossat, A. Amadio, M. Eder, J.M. Israel, S.H. Oliet, D.L. Voisin, Extracellular signal-regulated kinase

phosphorylation in forebrain neurones contributes to osmoregulatory mechanisms, J Physiol, 592 (2014) 1637-1654.

[22] H. Eilers, S.Y. Lee, C.W. Hau, A. Logvinova, M.A. Schumacher, The rat vanilloid receptor splice variant VR.5'sv blocks TRPV1 activation, Neuroreport, 18 (2007) 969-973.

[23] S. England, F. Heblich, I. James, J. Robbins, R. Docherty, Bradykinin evokes a Ca2+-activated chloride current in non-neuronal cells isolated from neonatal rat dorsal root ganglia., J Physiol, 530 (2001) 395-403.

[24] N. Fukumoto, N. Kitamura, K. Niimi, E. Takahashi, C. Itakura, I. Shibuya, Ca2+ channel currents in dorsal root ganglion neurons of P/Q-type voltage-gated Ca2+ channel mutant mouse, rolling mouse Nagoya, Neurosci Res, 73 (2012) 199-206.

[25] L. Gouzenes, N. Sabatier, P. Richard, F.C. Moos, G. Dayanithi, V1a- and V2-type vasopressin receptors mediate vasopressin-induced Ca2+ responses in isolated rat supraoptic neurones, J Physiol, 517 (Pt 3) (1999) 771-779.

[26] S.K. Han, V. Mancino, M.I. Simon, Phospholipase Cbeta 3 mediates the

scratching response activated by the histamine H1 receptor on C-fiber nociceptive neurons, Neuron, 52 (2006) 691-703.

[27] M. Hanani, Satellite glial cells in sensory ganglia: from form to function, Brain Res Brain Res Rev, 48 (2005) 457-476.

[28] A. Hassan, D. Mason, Mechanisms of desensitization of the adrenocorticotropin response to arginine vasopressin in ovine anterior pituitary cells, J Endocrinol, 184 (2005) 29-40.

[29] A. Hassan, S. Chacko, D. Mason, Desensitization of the adrenocorticotrophin responses to arginine vasopressin and corticotrophin-releasing hormone in ovine anterior pituitary cells, J Endocrinol, 178 (2003) 491-501.

[30] N.F. Holt, K.L. Haspel, Vasopressin: a review of therapeutic applications, Journal of cardiothoracic and vascular anesthesia, 24 (2010) 330-347.

[31] A. Horn, S. Lightman, Vasopressin-induced turnover of phosphatidylinositol in the sensory nervous system of the rat., Exp Brain

Res, 68 (1987) 299-304.

[32] A.M. Horn, S.L. Lightman, Vasopressin-induced turnover of phosphatidylinositol in the sensory nervous system of the rat, Exp Brain Res, 68 (1987) 299-304.

[33] K.R. Jessen, R. Mirsky, The origin and development of glial cells in peripheral nerves, Nat Rev Neurosci, 6 (2005) 671-682.

[34] E.K. Joseph, O. Bogen, N. Alessandri-Haber, J.D. Levine, PLC-beta 3 signals upstream of PKC epsilon in acute and chronic inflammatory hyperalgesia, Pain, 132 (2007) 67-73.

[35] J. Jung, S.Y. Lee, S.W. Hwang, H. Cho, J. Shin, Y.S. Kang, S. Kim, U. Oh, Agonist recognition sites in the cytosolic tails of vanilloid receptor 1, J Biol Chem, 277 (2002) 44448-44454.

[36] M. Kai-Kai, B. Anderton, P. Keen, A quantitative analysis of the interrelationships between subpopulations of rat sensory neurons containing arginine vasopressin or oxytocin and those containing substance P, fluoride-resistant acid phosphatase or neurofilament protein., Neuroscience,

18 (1986) 475-486.

[37] M.A. Kai-Kai, B.H. Anderton, P. Keen, A quantitative analysis of the interrelationships between subpopulations of rat sensory neurons containing arginine vasopressin or oxytocin and those containing substance P, fluoride-resistant acid phosphatase or neurofilament protein, Neuroscience, 18 (1986) 475-486.

[38] T. Karashima, Effects of vasopressin on smooth muscle cells of guinea-pig mesenteric vessels, Br J Pharmacol, 72 (1981) 673-684.

[39] N. Kitamura, A. Konno, T. Kuwahara, Y. Komagiri, Nerve growth factor-induced hyperexcitability of rat sensory neuron in culture, Biomed Res, 26 (2005) 123-130.

[40] Y. Komagiri, N. Kitamura, Effect of intracellular dialysis of ATP on the hyperpolarization-activated cation current in rat dorsal root ganglion neurons, Journal of neurophysiology, 90 (2003) 2115-2122.

[41] Y. Komori, M. Tanaka, M. Kuba, M. Ishii, M. Abe, N. Kitamura, A. Verkhratsky, I. Shibuya, G. Dayanithi, Ca(2+) homeostasis, Ca(2+)

signalling and somatodendritic vasopressin release in adult rat supraoptic nucleus neurones, Cell Calcium, 48 (2010) 324-332.

[42] T.A. Koshimizu, K. Nakamura, N. Egashira, M. Hiroyama, H. Nonoguchi, A. Tanoue, Vasopressin V1a and V1b receptors: from molecules to physiological systems, Physiol Rev, 92 (2012) 1813-1864.

[43] J. Lagercrantz, F. Piehl, M. Nordenskjold, C. Larsson, G. Weber, Expression of the phosphoinositide-specific phospholipase Cbeta3 gene in the rat, Neuroreport, 6 (1995) 2542-2544.

[44] N. Le Douarin, C. Dulac, E. Dupin, P. Cameron-Curry, Glial cell lineages in the neural crest, Glia, 4 (1991) 175-184.

[45] S. Lechner, H. Frenzel, R. Wang, G. Lewin, Developmental waves of mechanosensitivity acquisition in sensory neuron subtypes during embryonic development., EMBO J, 28 (2009) 1479-1491.

[46] S.G. Lechner, S. Markworth, K. Poole, E.S. Smith, L. Lapatsina, S. Frahm, M. May, S. Pischke, M. Suzuki, I. Ibanez-Tallon, F.C. Luft, J. Jordan, G.R. Lewin, The molecular and cellular identity of peripheral osmoreceptors,

Neuron, 69 (2011) 332-344.

[47] C. Lee, M. Watkins, J. Patterson, W. Gattis, C. O'connor, M. Gheorghiade, K.J. Adams, Vasopressin: a new target for the treatment of heart failure., Am Heart J, 146 (2003) 9-18.

[48] G. Leng, W.T. Mason, R.G. Dyer, The supraoptic nucleus as an osmoreceptor, Neuroendocrinology, 34 (1982) 75-82.

[49] Y. Li, A.J. Shiels, G. Maszak, K.L. Byron, Vasopressin-stimulated Ca2+ spiking in vascular smooth muscle cells involves phospholipase D, Am J Physiol Heart Circ Physiol, 280 (2001) H2658-2664.

[50] W. Liedtke, J.M. Friedman, Abnormal osmotic regulation in trpv4-/- mice, Proc Natl Acad Sci U S A, 100 (2003) 13698-13703.

[51] H. Link, G. Dayanithi, K. Föhr, M. Gratzl, Oxytocin at physiological concentrations evokes adrenocorticotropin (ACTH) release from corticotrophs by increasing intracellular free calcium mobilized mainly from intracellular stores. Oxytocin displays synergistic or additive effects on ACTH-releasing factor or arginine vasopressin-induced ACTH secretion,

respectively., Endocrinology, 130 (1992) 2183-2191.

[52] K. Machida, S. Wakamatsu, Y. Izumi, T. Yosifovska, T. Matsuzaki, Y. Nakayama, Y. Kohda, T. Inoue, H. Saito, K. Tomita, H. Nonoguchi, Downregulation of the V2 vasopressin receptor in dehydration: mechanisms and role of renal prostaglandin synthesis, Am J Physiol Renal Physiol, 292 (2007) F1274-1282.

[53] S. Madduri, B. Gander, Schwann cell delivery of neurotrophic factors for peripheral nerve regeneration, J Peripher Nerv Syst, 15 (2010) 93-103.

[54] M. Manning, S. Stoev, B. Chini, T. Durroux, B. Mouillac, G. Guillon, Peptide and non-peptide agonists and antagonists for the vasopressin and oxytocin V1a, V1b, V2 and OT receptors: research tools and potential therapeutic agents., Prog Brain Res, 170 (2008) 473-512.

[55] W.T. Mason, Supraoptic neurones of rat hypothalamus are osmosensitive, Nature, 287 (1980) 154-157.

[56] K.E. Miller, B.A. Richards, R.M. Kriebel, Glutamine-, glutamine synthetase-, glutamate dehydrogenase- and pyruvate

carboxylase-immunoreactivities in the rat dorsal root ganglion and peripheral nerve, Brain Res, 945 (2002) 202-211.

[57] A. Mizuno, N. Matsumoto, M. Imai, M. Suzuki, Impaired osmotic sensation in mice lacking TRPV4, Am J Physiol Cell Physiol, 285 (2003) C96-101.

[58] T.P. Nedungadi, F.R. Carreno, J.D. Walch, C.S. Bathina, J.T. Cunningham, Region-specific changes in transient receptor potential vanilloid channel expression in the vasopressin magnocellular system in hepatic cirrhosis-induced hyponatraemia, J Neuroendocrinol, 24 (2012) 642-652.

[59] E. Nishihara, T.Y. Hiyama, M. Noda, Osmosensitivity of transient receptor potential vanilloid 1 is synergistically enhanced by distinct activating stimuli such as temperature and protons, PLoS One, 6 (2011) e22246.

[60] U. Oh, S.W. Hwang, D. Kim, Capsaicin activates a nonselective cation channel in cultured neonatal rat dorsal root ganglion neurons, J Neurosci, 16

(1996) 1659-1667.

[61] P.T. Ohara, J.P. Vit, A. Bhargava, M. Romero, C. Sundberg, A.C. Charles, L. Jasmin, Gliopathic pain: when satellite glial cells go bad, Neuroscientist, 15 (2009) 450-463.

[62] S.H. Oliet, C.W. Bourque, Mechanosensitive channels transduce osmosensitivity in supraoptic neurons, Nature, 364 (1993) 341-343.

[63] C. Orlandi, L. La Via, D. Bonini, C. Mora, I. Russo, A. Barbon, S. Barlati, AMPA receptor regulation at the mRNA and protein level in rat primary cortical cultures, PLoS One, 6 (2011) e25350.

[64] Y. Ozaki, N. Kitamura, A. Tsutsumi, G. Dayanithi, I. Shibuya, NGF-induced hyperexcitability causes spontaneous fluctuations of intracellular Ca2+ in rat nociceptive dorsal root ganglion neurons., Cell Calcium, 45 (2009) 209-215.

[65] Y. Ozaki, N. Kitamura, A. Tsutsumi, G. Dayanithi, I. Shibuya, NGF-induced hyperexcitability causes spontaneous fluctuations of intracellular Ca2+ in rat nociceptive dorsal root ganglion neurons, Cell

Calcium, 45 (2009) 209-215.

[66] E. Pannese, The satellite cells of the sensory ganglia, Adv Anat Embryol Cell Biol, 65 (1981) 1-111.

[67] A.B. Parekh, J.W. Putney, Jr., Store-operated calcium channels, Physiol Rev, 85 (2005) 757-810.

[68] V. Parpura, F. Liu, K. Jeftinija, P. Haydon, S. Jeftinija, Neuroligand-evoked calcium-dependent release of excitatory amino acids from Schwann cells., J Neurosci, 15 (1995) 5831-5839.

[69] E.A. Popenoe, V. Du Vigneaud, A partial sequence of amino acids in performic acid-oxidized vasopressin, J Biol Chem, 206 (1954) 353-360.

[70] L.S. Premkumar, S. Agarwal, D. Steffen, Single-channel properties of native and cloned rat vanilloid receptors, J Physiol, 545 (2002) 107-117.

[71] M. Raisinghani, R.M. Pabbidi, L.S. Premkumar, Activation of transient receptor potential vanilloid 1 (TRPV1) by resiniferatoxin, J Physiol, 567 (2005) 771-786.

[72] D. Richard, C.W. Bourque, Synaptic control of rat supraoptic neurones

during osmotic stimulation of the organum vasculosum lamina terminalis in vitro, J Physiol, 489 (Pt 2) (1995) 567-577.

[73] A.R. Rutter, Q.P. Ma, M. Leveridge, T.P. Bonnert, Heteromerization and colocalization of TrpV1 and TrpV2 in mammalian cell lines and rat dorsal root ganglia, Neuroreport, 16 (2005) 1735-1739.

[74] N. Sabatier, P. Richard, G. Dayanithi, Activation of multiple intracellular transduction signals by vasopressin in vasopressin-sensitive neurones of the rat supraoptic nucleus, J Physiol, 513 (Pt 3) (1998) 699-710.

[75] N. Sabatier, I. Shibuya, G. Dayanithi, Intracellular calcium increase and somatodendritic vasopressin release by vasopressin receptor agonists in the rat supraoptic nucleus: involvement of multiple intracellular transduction signals, J Neuroendocrinol, 16 (2004) 221-236.

[76] R.W. Schrier, V. Briner, C. Caramelo, Cellular action and interactions of arginine vasopressin in vascular smooth muscle: mechanisms and clinical implications, J Am Soc Nephrol, 4 (1993) 2-11.

[77] M.A. Schumacher, I. Moff, S.P. Sudanagunta, J.D. Levine, Molecular

cloning of an N-terminal splice variant of the capsaicin receptor. Loss of N-terminal domain suggests functional divergence among capsaicin receptor subtypes, J Biol Chem, 275 (2000) 2756-2762.

[78] R.S. Scroggs, A.P. Fox, Calcium current variation between acutely isolated adult rat dorsal root ganglion neurons of different size, J Physiol, 445 (1992) 639-658.

[79] N.W. Seidler, I. Jona, M. Vegh, A. Martonosi, Cyclopiazonic acid is a specific inhibitor of the Ca2+-ATPase of sarcoplasmic reticulum, J Biol Chem, 264 (1989) 17816-17823.

[80] R. Sharif Naeini, M.F. Witty, P. Seguela, C.W. Bourque, An N-terminal variant of Trpv1 channel is required for osmosensory transduction, Nat Neurosci, 9 (2006) 93-98.

[81] T.J. Shi, S.X. Liu, H. Hammarberg, M. Watanabe, Z.Q. Xu, T. Hokfelt, Phospholipase C{beta}3 in mouse and human dorsal root ganglia and spinal cord is a possible target for treatment of neuropathic pain, Proc Natl Acad Sci U S A, 105 (2008) 20004-20008.

[82] S. Shim, G.L. Ming, Roles of channels and receptors in the growth cone during PNS axonal regeneration, Exp Neurol, 223 (2010) 38-44.

[83] R.J. Smith, L.M. Sam, J.M. Justen, G.L. Bundy, G.A. Bala, J.E. Bleasdale, Receptor-coupled signal transduction in human polymorphonuclear neutrophils: effects of a novel inhibitor of phospholipase C-dependent processes on cell responsiveness, J Pharmacol Exp Ther, 253 (1990) 688-697.

[84] M. Steiner, M.I. Phillips, Renal tubular vasopressin receptors downregulated by dehydration, Am J Physiol, 254 (1988) C404-410.

[85] J.R. Sudbury, S. Ciura, R. Sharif-Naeini, C.W. Bourque, Osmotic and thermal control of magnocellular neurosecretory neurons--role of an N-terminal variant of trpv1, Eur J Neurosci, 32 (2010) 2022-2030.

[86] M. Suzuki, J. Sato, K. Kutsuwada, G. Ooki, M. Imai, Cloning of a stretch-inhibitable nonselective cation channel, J Biol Chem, 274 (1999) 6330-6335.

[87] N. Syed, C.A. Martens, W.H. Hsu, Arginine vasopressin increases

glutamate release and intracellular Ca2+ concentration in hippocampal and cortical astrocytes through two distinct receptors, J Neurochem, 103 (2007) 229-237.

[88] Y. Terada, K. Tomita, H. Nonoguchi, T. Yang, F. Marumo, Different localization and regulation of two types of vasopressin receptor messenger RNA in microdissected rat nephron segments using reverse transcription polymerase chain reaction, J Clin Invest, 92 (1993) 2339-2345.

[89] R. Thul, T. Bellamy, H. Roderick, M. Bootman, S. Coombes, Calcium oscillations., Adv Exp Med Biol, 641 (2008) 1-27.

[90] W. Tian, Y. Fu, D.H. Wang, D.M. Cohen, Regulation of TRPV1 by a novel renally expressed rat TRPV1 splice variant, Am J Physiol Renal Physiol, 290 (2006) F117-126.

[91] V.A. Tobin, H. Hashimoto, D.W. Wacker, Y. Takayanagi, K. Langnaese, C. Caquineau, J. Noack, R. Landgraf, T. Onaka, G. Leng, S.L. Meddle, M. Engelmann, M. Ludwig, An intrinsic vasopressin system in the olfactory bulb is involved in social recognition, Nature, 464 (2010) 413-417.

[92] Y. Ueta, H. Fujihara, R. Serino, G. Dayanithi, H. Ozawa, K. Matsuda, M. Kawata, J. Yamada, S. Ueno, A. Fukuda, D. Murphy, Transgenic expression of enhanced green fluorescent protein enables direct visualization for physiological studies of vasopressin neurons and isolated nerve terminals of the rat, Endocrinology, 146 (2005) 406-413.

[93] P.G. Vallet, A.J. Baertschi, Spinal afferents for peripheral osmoreceptors in the rat, Brain Res, 239 (1982) 271-274.

[94] V. Van Putten, X. Li, J. Maselli, R.A. Nemenoff, Regulation of smooth muscle alpha-actin promoter by vasopressin and platelet-derived growth factor in rat aortic vascular smooth muscle cells, Circ Res, 75 (1994) 1126-1130.

[95] J.A. Vega, M.E. del Valle-Soto, B. Calzada, J.C. Alvarez-Mendez, Immunohistochemical localization of S-100 protein subunits (alpha and beta) in dorsal root ganglia of the rat, Cell Mol Biol, 37 (1991) 173-181.

[96] J.G. Verbalis, How does the brain sense osmolality?, J Am Soc Nephrol, 18 (2007) 3056-3059.

[97] C. Viero, I. Shibuya, N. Kitamura, A. Verkhratsky, H. Fujihara, A. Katoh, Y. Ueta, H.H. Zingg, A. Chvatal, E. Sykova, G. Dayanithi, REVIEW: Oxytocin: Crossing the Bridge between Basic Science and Pharmacotherapy, CNS Neurosci Ther, 16 e138-e156.

[98] C. Viero, I. Shibuya, N. Kitamura, A. Verkhratsky, H. Fujihara, A. Katoh, Y. Ueta, H.H. Zingg, A. Chvatal, E. Sykova, G. Dayanithi, REVIEW: Oxytocin: Crossing the bridge between basic science and pharmacotherapy, CNS Neurosci Ther, 16 (2010) e138-156.

[99] J.P. Vit, P.T. Ohara, A. Bhargava, K. Kelley, L. Jasmin, Silencing the Kir4.1 potassium channel subunit in satellite glial cells of the rat trigeminal ganglion results in pain-like behavior in the absence of nerve injury, J Neurosci, 28 (2008) 4161-4171.

[100] S. Volpi, C. Rabadan-Diehl, G. Aguilera, Vasopressinergic regulation of the hypothalamic pituitary adrenal axis and stress adaptation, Stress, 7 (2004) 75-83.

[101] Z. Winter, A. Buhala, F. Otvos, K. Josvay, C. Vizler, G. Dombi, G.

Szakonyi, Z. Olah, Functionally important amino acid residues in the transient receptor potential vanilloid 1 (TRPV1) ion channel--an overview of the current mutational data, Mol Pain, 9 (2013) 30.

[102] S. Yibchok-Anun, H. Cheng, P. Heine, W. Hsu, Characterization of receptors mediating AVP- and OT-induced glucagon release from the rat pancreas., Am J Physiol, 277 (1999) E56-62.

[103] T. Yokoyama, T. Saito, T. Ohbuchi, H. Hashimoto, H. Suzuki, H. Otsubo, H. Fujihara, T. Nagatomo, Y. Ueta, TRPV1 gene deficiency attenuates miniature EPSC potentiation induced by mannitol and angiotensin II in supraoptic magnocellular neurons, J Neurosci, 30 (2010) 876-884.

[104] Z. Zhang, C.W. Bourque, Calcium permeability and flux through osmosensory transduction channels of isolated rat supraoptic nucleus neurons, Eur J Neurosci, 23 (2006) 1491-1500.

SUMMARY

【INTRODUCTION・PURPOSE】 Arginine vasopressin (AVP) is a neuropeptide synthesized in the cell bodies of the magnocellular neurosecretory cells (MNCs) and parvocellular neurosecretory cells in the supraoptic nucleus (SON) and the paraventricular nucleus in the hypothalamus. AVP is known to play a crucial role in maintaining the osmolality and volume of the body fluid. It has been argued that MNCs in the SON possess intrinsic osmosensing mechanisms, which are lost in transient receptor potential vanilloid 1 (*Trpv1*)-knock-out mice. The molecular identity of the osmoreceptors expressed in MNCs is believed to be associated with the N-terminal splice variants of *Trpv1*, however, their entire molecular structures have not been identified. The purpose of the Chapter 1 was to uncover the structure and function of molecules related to the central osmoreceptor in the rat SON. RT-PCR and immunohistochemistry were performed for TRPV1-related molecules, and electrophysiological parameters and intracellular Ca^{2+} concentration ($[Ca^{2+}]_i$) in rat SON neurons were measured in response to osmolality changes and TRPV-related drugs.

Besides its function in the osmolality regulation, AVP has been shown to exert other important physiological functions in the central and peripheral nervous systems. In the dorsal root ganglion (DRG), it has been reported that AVP-like immunoreactivity is detected in the DRG neurons and exposure to AVP induced phosphatidylinositol turnover in the DRG. In the Chapter 2, AVP-induced responses in rat DRG cells were investigated using $[Ca^{2+}]_i$ imaging, immunohistochemistry and RT-PCR.

【RESULTS・DISCUSSION】 In the Chapter 1, RT-PCR analysis revealed full-length *Trpv1* and a new N-terminal splice variant, *Trpv1_SON* (LC008303) in the rat SON. Positive immunostaining was observed using an antibody against the N-terminal portion of TRPV1 in arginine vasopressin (AVP)-immunoreactive neurons, but not in oxytocin (OT)-immunoreactive neurons. Approximately 20% of SON neurons responded to 50 mM mannitol (+30 mOsml/kg), with $[Ca^{2+}]_i$ increases. Mannitol-induced responses were observed in AVP neurons isolated from AVP-eGFP transgenic rats and identified by GFP fluorescence, but not in OT neurons isolated from OT-mRFP transgenic rats

and identified by RFP fluorescence. The mannitol-induced $[Ca^{2+}]_i$ responses were reversibly blocked by the non-selective TRPV antagonist, ruthenium red (10 μM) and the selective TRPV1 antagonists, capsazepine (10 μM) and BCTC (10 μM). These antagonists had little or no effect on K^+-induced $[Ca^{2+}]_i$ responses. Mannitol-induced increases in the frequency of action potentials were reversibly suppressed by capsazepine (10 μM). Although the TRPV1 agonist, capsaicin (100 nM) evoked no response at room temperature, it triggered cationic currents when the temperature was increased to 36 ºC, and the reversal potential (E_{rev}) was -46.4 ± 4.1 mV, which is close to the reported E_{rev} of hyperosmolality-induced current in rat SON, but different from E_{rev} of capsaicin-induced currents recorded in rat DRG neurons or TRPV1-expressing cells. Although the I-V relation of capsaicin-induced currents reported in DRG neurons or TRPV1-expressing cells showed evident outward rectification, that observed in SON neurons was ohmic, Capsaicin (100 nM) caused only a minute $[Ca^{2+}]_i$ increase (8.5 ± 2.7 nM) in nine SON neurons that responded to mannitol (50 mM) with a large $[Ca^{2+}]_i$ transients (135 ± 15 nM) at 24 ºC. In contrast, capsaicin (100 nM) evoked significant $[Ca^{2+}]_i$ elevations (134 ± 14 nM) at 36 ºC in all the nine SON neurons.

Capsaicin-induced $[Ca^{2+}]_i$ increases were reversibly blocked by capsazepine (10 μM).

In the Chapter 2, $[Ca^{2+}]_i$ measurements showed that AVP evoked $[Ca^{2+}]_i$ responses in non-neuronal cells in a concentration-dependent manner (100 pM to 1 μM). The amplitude of the $[Ca^{2+}]_i$ responses increased with days *in vitro* in culture, reaching a maximum amplitude after 4-5 days. Immunostaining by anti-S-100 antibody revealed that more than 70% of S-100 positive cells were AVP-responsive, indicating that glial cells responded to AVP and increased their $[Ca^{2+}]_i$. The responses were inhibited by depletion of the intracellular Ca^{2+} stores by the inhibitor of the Ca^{2+}-ATPase expressed on the endo/sarcoplasmic reticulum, cyclopiazonic acid (10 mM), or in the presence of the inhibitor of phospholipase C, U73122 (1 μM), indicating that the responses are mediated by a metabotropic mechanism involving inositol trisphosphate ($InsP_3$). The AVP-evoked responses were blocked by the specific blockers for V_1 receptors, $(d(CH_2)_5{}^1,Tyr(Me)^2,Arg^8)$-Vasopressin, but unaffected by the OT receptor blocker, $(d(CH_2)_5{}^1,Tyr(Me)^2,Thr^4,Orn^8,des\text{-}Gly\text{-}NH_2{}^9)$-Vasotocin. Moreover, V_{1a} but not V_{1b} receptor mRNA was expressed sustainably through the culture period in cultured DRG cells.

【**CONCLUSION**】The results in the Chapter 1 suggest that AVP neurons in the rat SON possess functional full-length TRPV1. Moreover, differences between the responses to capsaicin or hyperosmolality obtained in rat SON neurons and those obtained from DRG neurons or TRPV1-expressing cells indicate that the osmoreceptor expressed in the SON may be a heterotetramer, in which TRPV1 is co-assembled with some other, yet unidentified, molecules.

The results in the Chapter 2 indicate that AVP induces a $[Ca^{2+}]_i$ increase involving an $InsP_3$-evoked release of Ca^{2+} from intracellular stores in rat DRG glial cells through their AVP V_{1a} receptor.